Supporting Information

Synthesis and Coordination Ability of the first Phosphavinyl(selenoxo)phosphorane: an Electronic Story.

Iulia-Andreea Aghion[1], Raluca A. Septelean[2]*, David Lucaci[2], Ionut-Tudor Moraru[2], Albert P. Soran[3], Catalin C. Ciocan[2], Emilia Licarete[4], Manuela Banciu[4], Gabriela Nemes[2]*

1. Faculty of Chemistry and Chemical Engineering, Doctoral School of Chemistry, Babes-Bolyai University, Cluj-Napoca 400028, Romania
2. Faculty of Chemistry and Chemical Engineering, Department of Chemistry, Babes-Bolyai University, Cluj-Napoca 400028, Romania
3. Faculty of Chemistry and Chemical Engineering, Department of Chemistry, Supramolecular Organic and Organometallic Chemistry Centre (SOOMCC), Babes-Bolyai University, Cluj-Napoca 400028, Romania
4. Faculty of Biology and Geology, Babes-Bolyai University, Cluj-Napoca 400028, Romania

*E-mail addresses:

raluca.septelean@ubbcluj.ro

gabriela.nemes@ubbcluj.ro

Contents

1. Experimental part

1. NMR spectra

1.1. Mes*P=C(Cl)-P(=Se)(*i*-Pr)$_2$ **(1)**

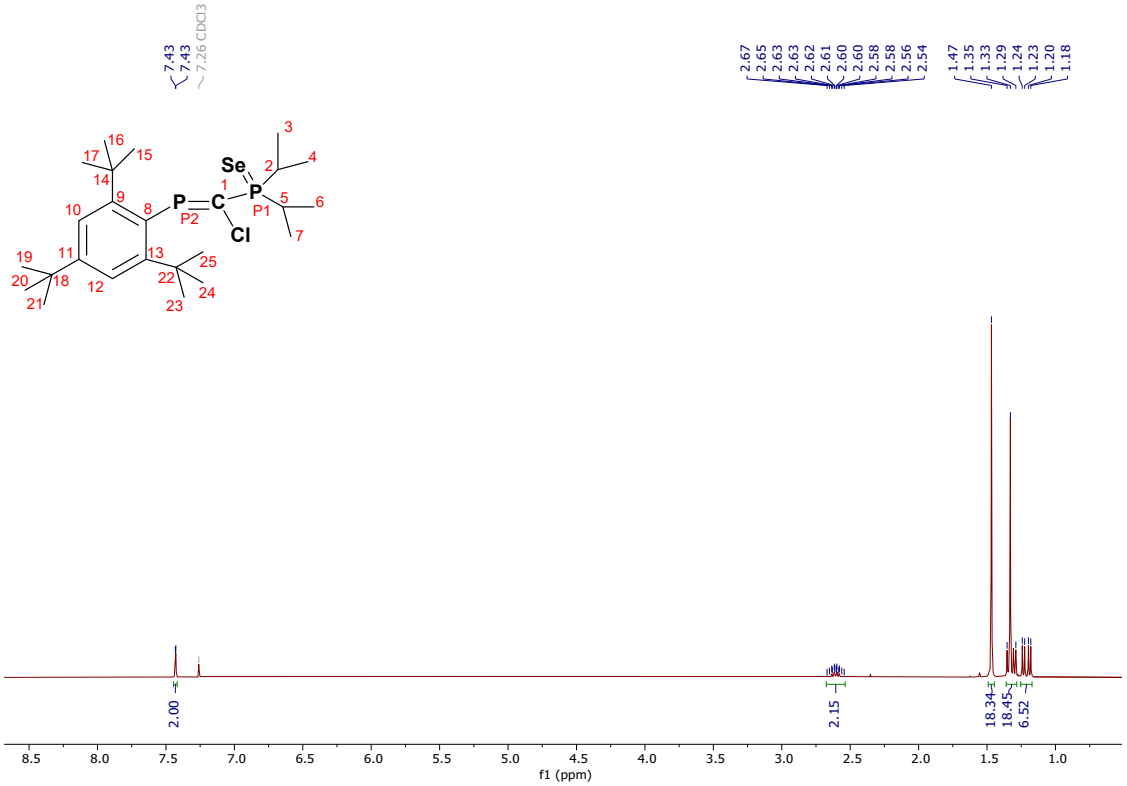

Figure S1. ^{1}H NMR spectrum of **1** in $CDCl_3$ (400.13 MHz).

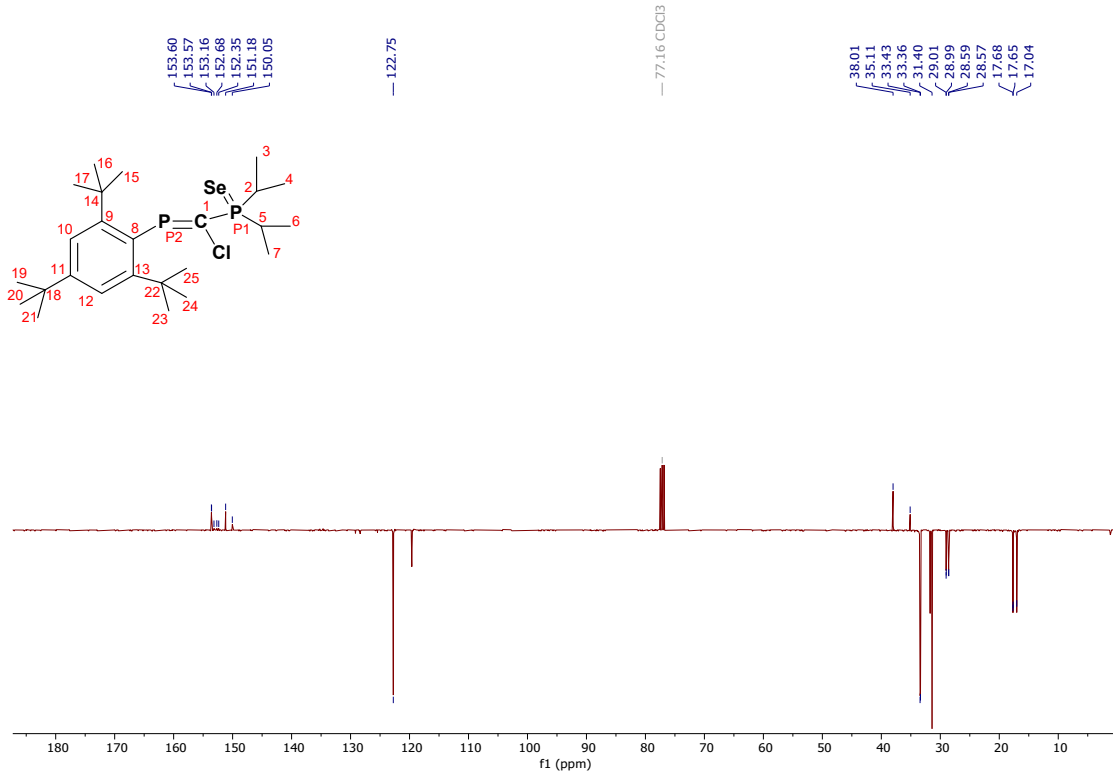

Figure S2. ^{13}C NMR spectrum of **1** in $CDCl_3$ (100.62 MHz).

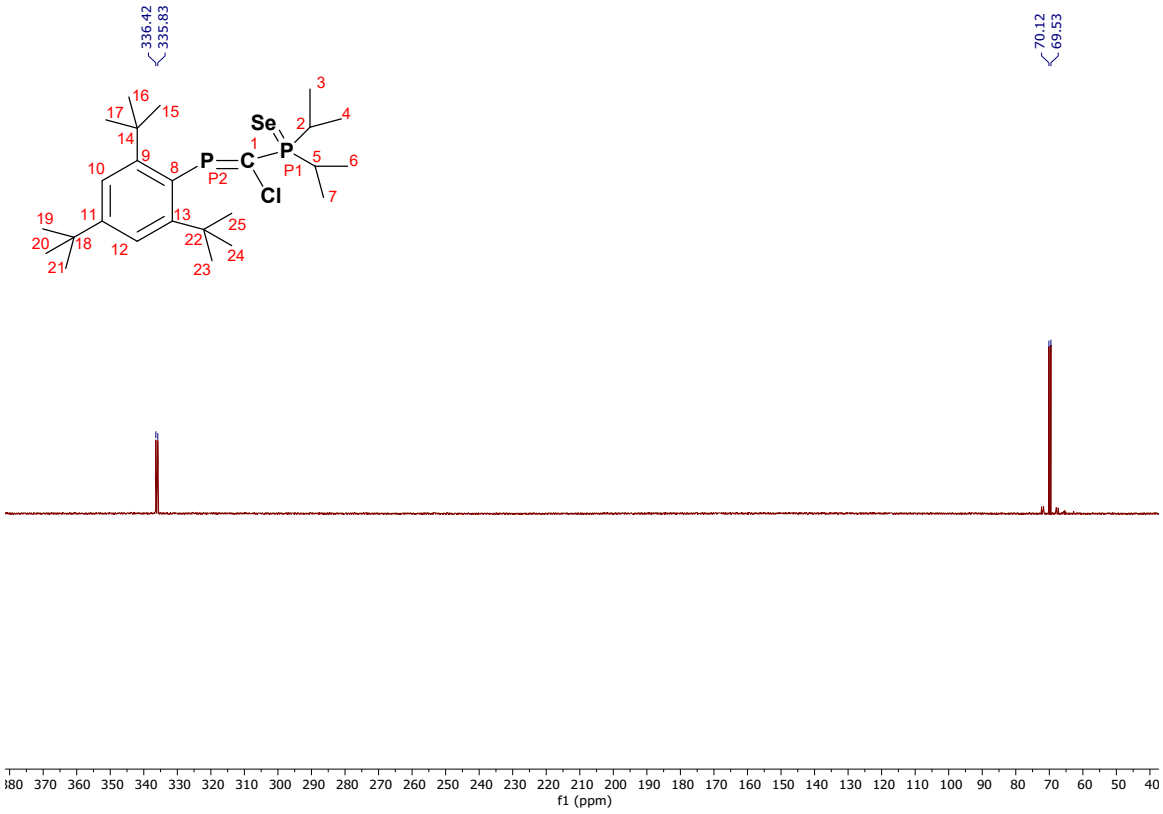

Figure S3. $^{31}P\{H\}$ NMR spectrum of **1** in $CDCl_3$ (162.00 MHz).

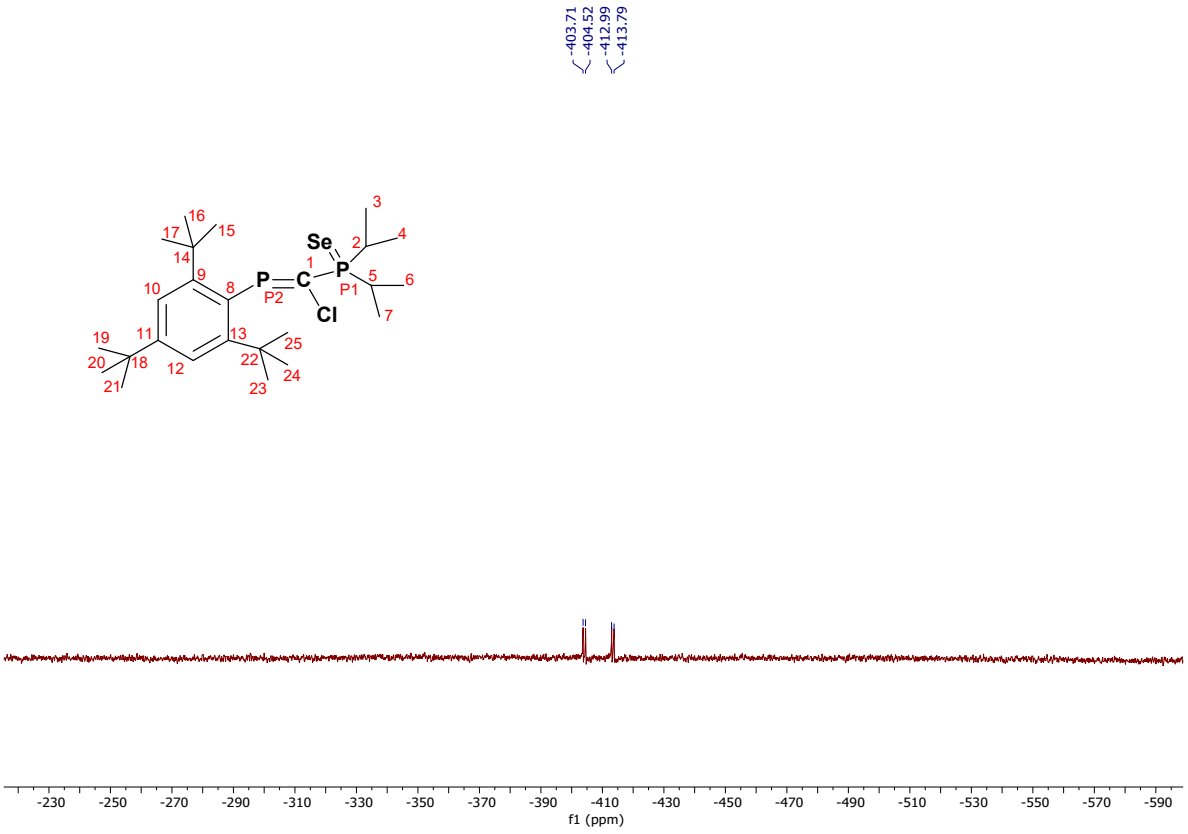

Figure S4. $^{77}Se\{H\}$ spectrum of **1** in $CDCl_3$ (76.31 MHz).

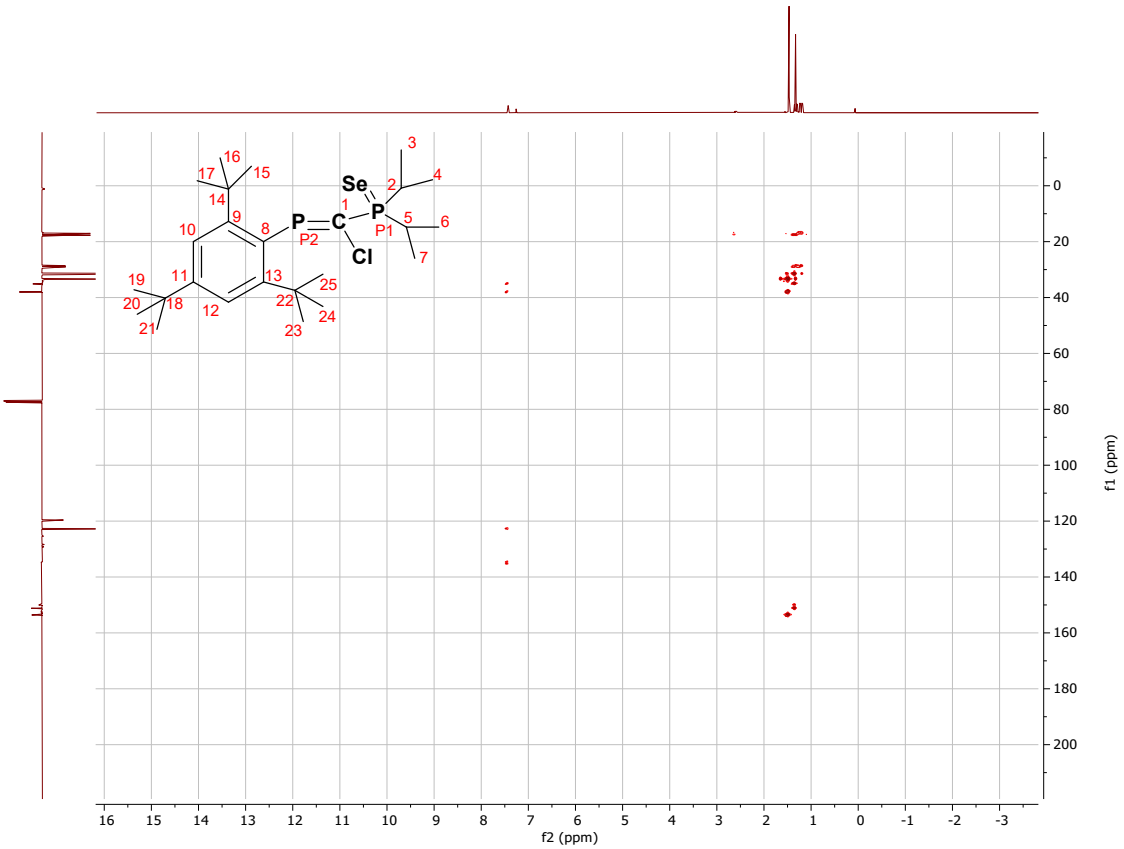

Figure S5. ^{1}H-^{13}C HMBC spectrum of **1** in $CDCl_3$ (400.13, 100.62MHz).

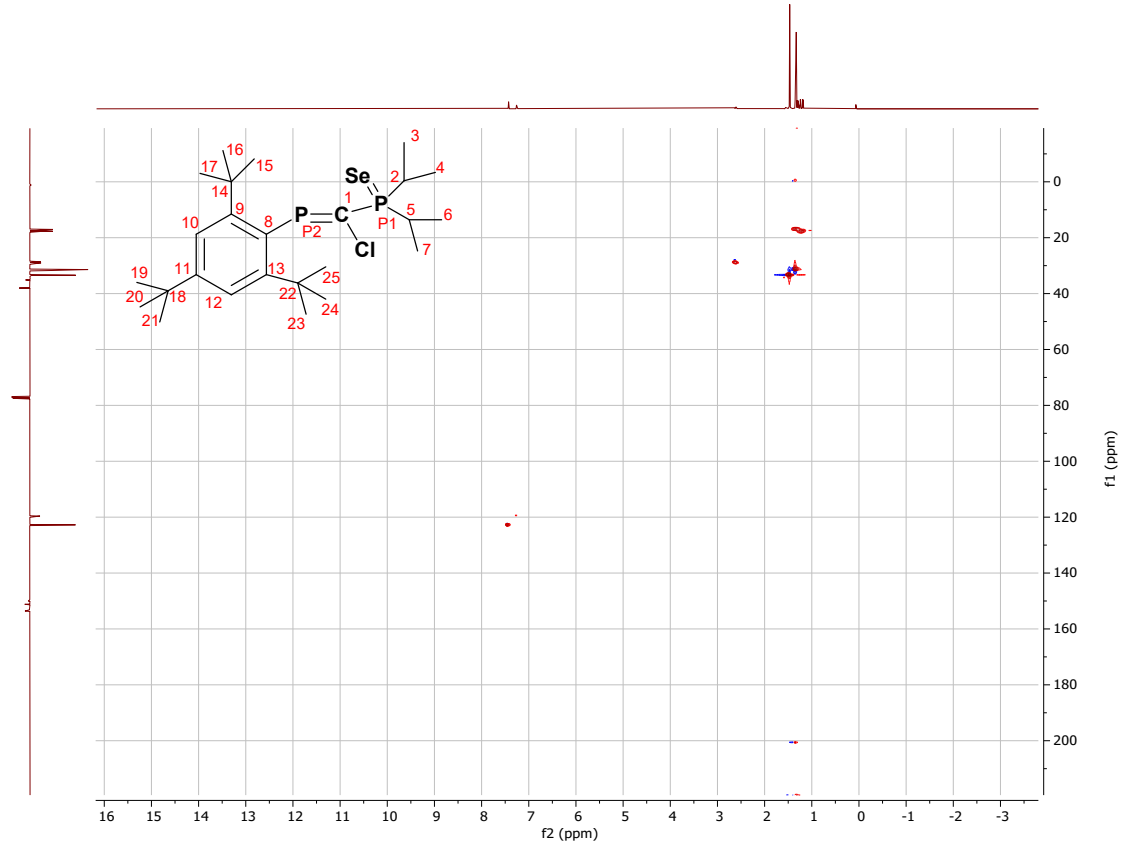

Figure S6. ^{1}H-^{13}C HSQC spectrum of **1** in $CDCl_3$ (400.13, 100.62MHz).

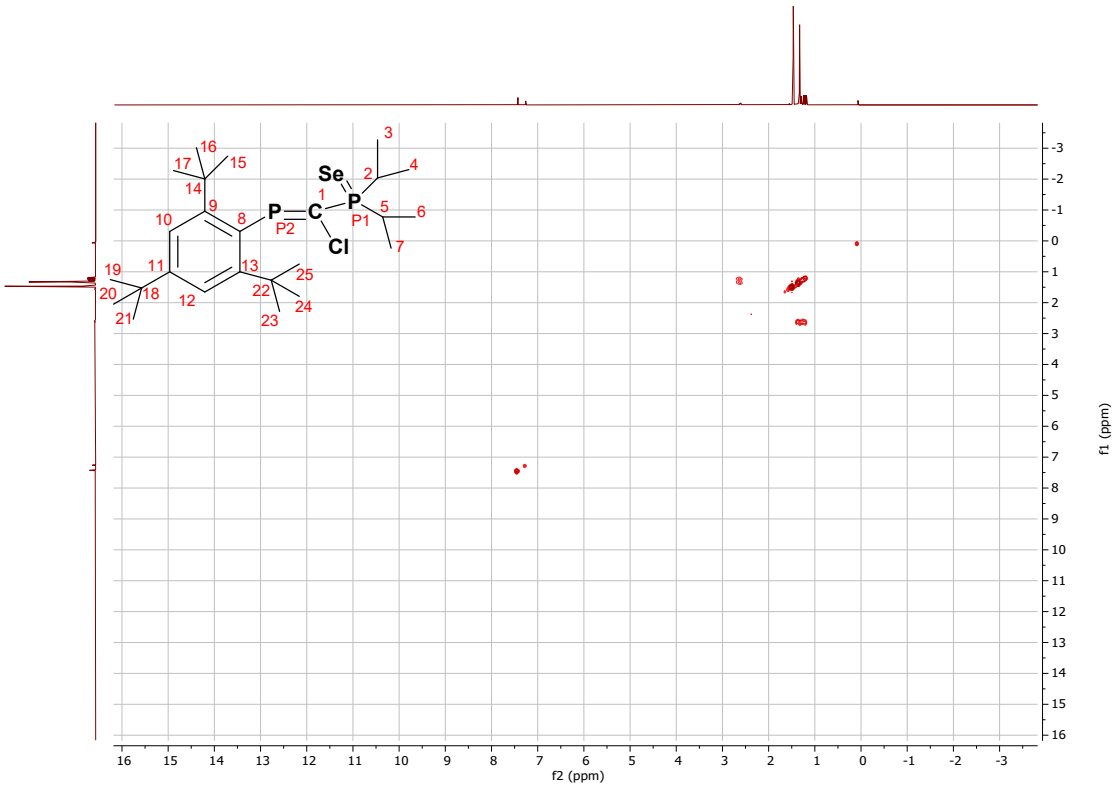

Figure S7. ^{1}H-^{1}H COSY spectrum of **1** in $CDCl_3$ (400.13, 400.13 MHz).

1.2. {Mes*P=C(Cl)-P(=Se)(*i*-Pr)$_2$}AuCl **(2)**

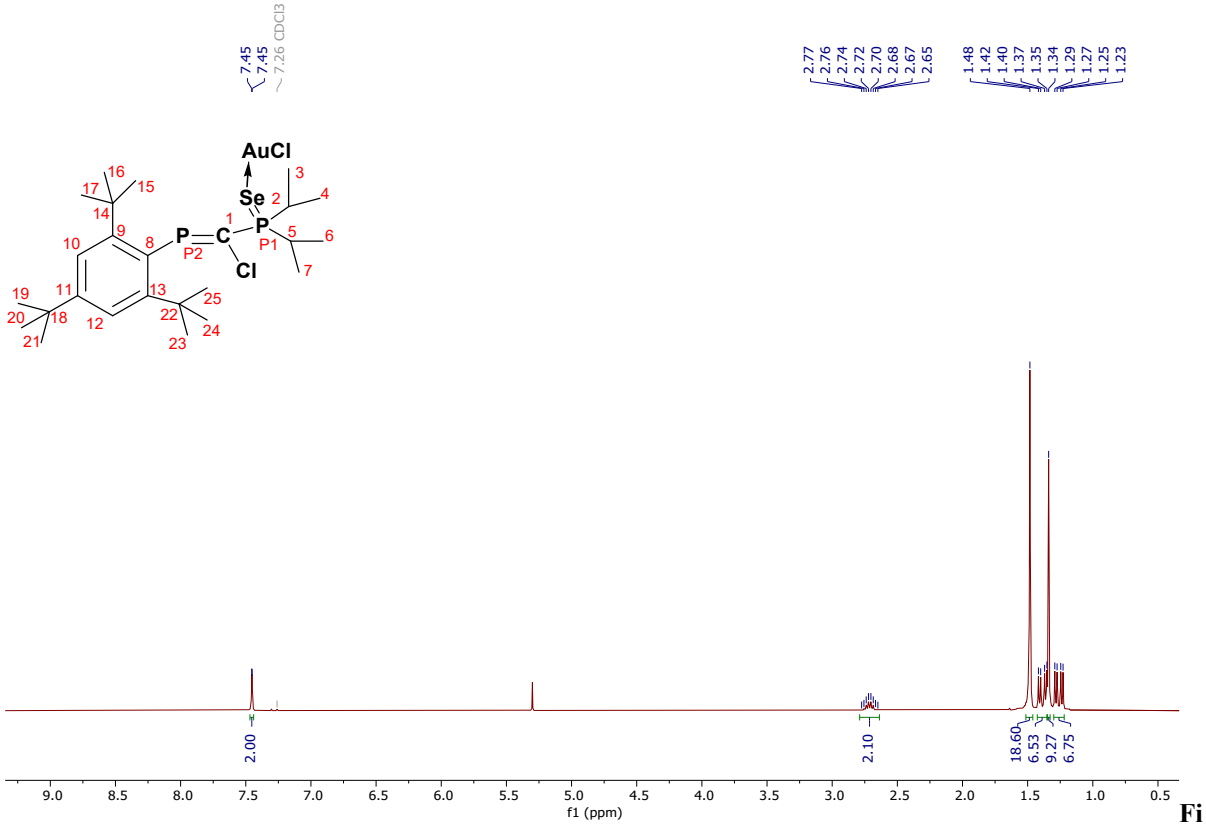

Figure S8. ^{1}H NMR spectrum of **2** in $CDCl_3$ (400.13 MHz).

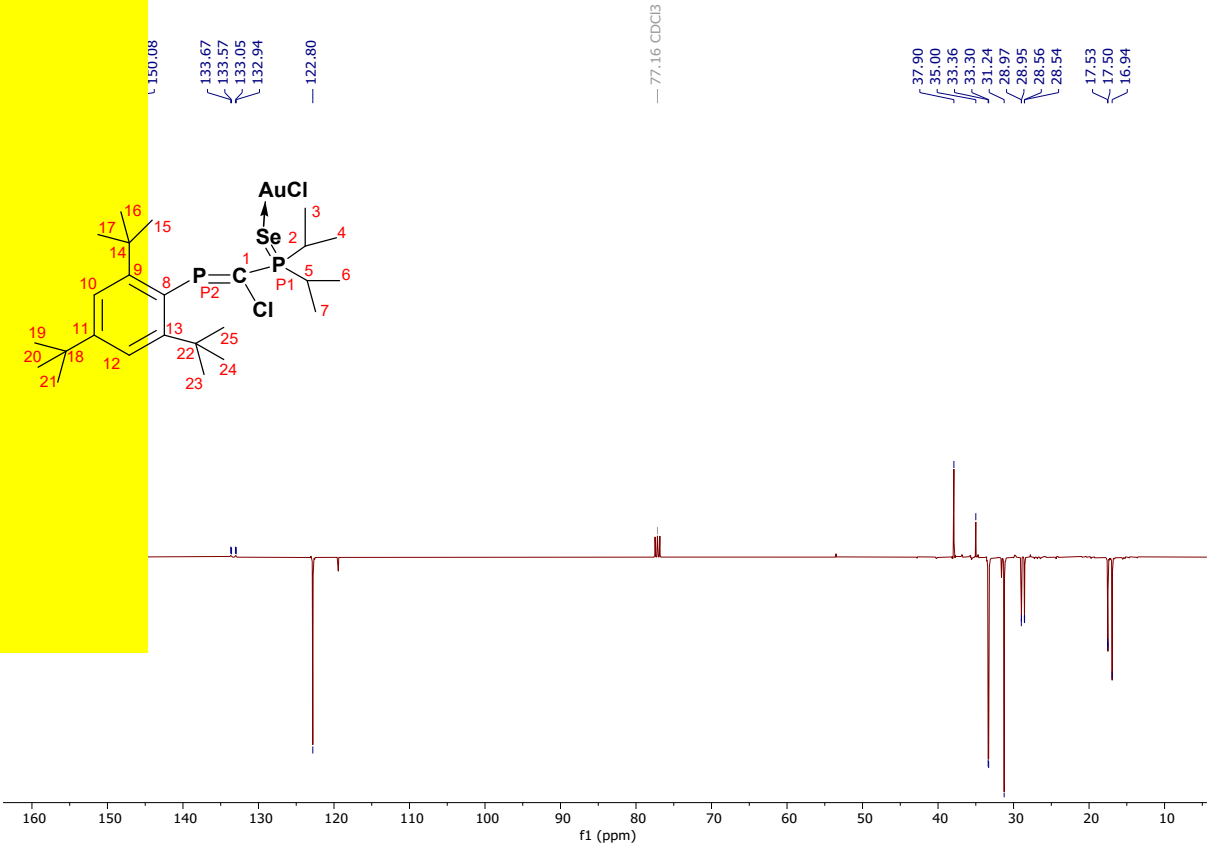

Figure S9. ^{13}C NMR spectrum of **2** in $CDCl_3$ (100.62 MHz).

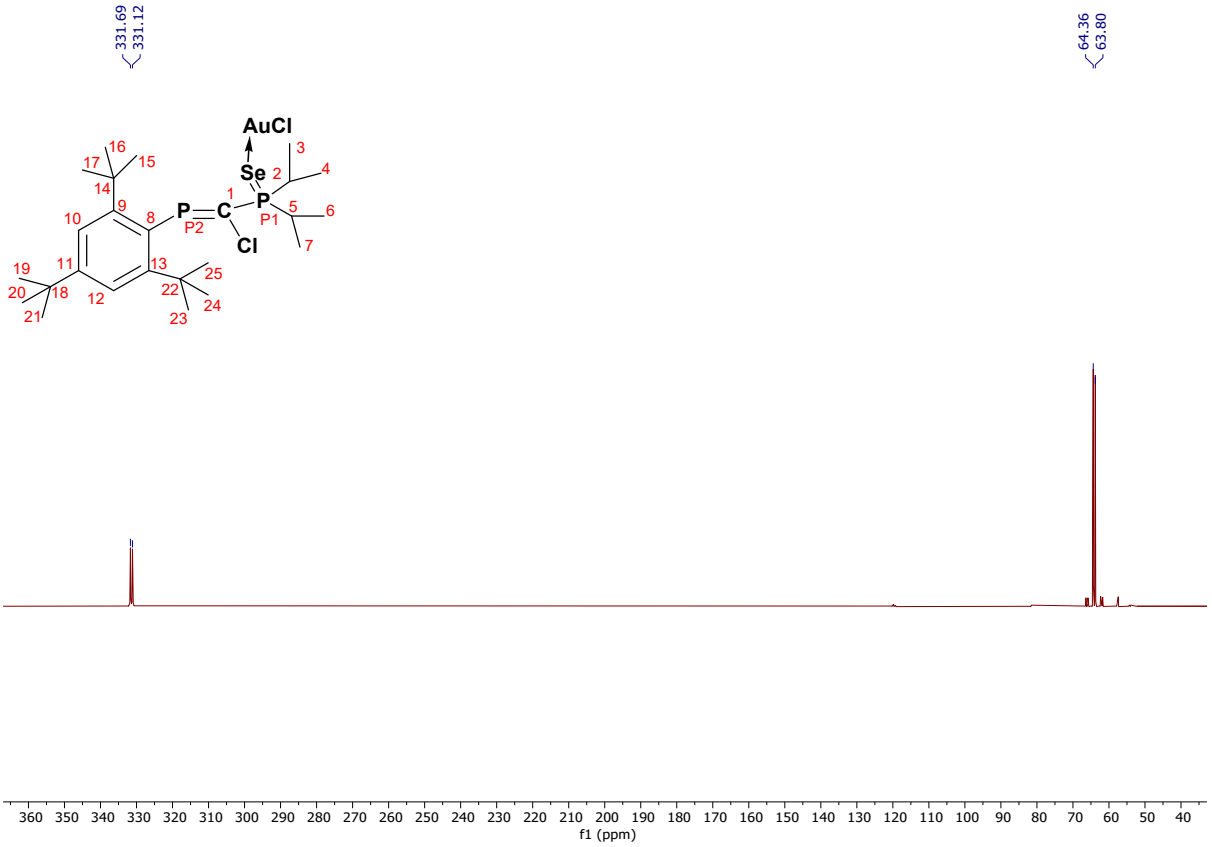

Figure S10a. $^{31}P\{H\}$ NMR spectrum of **2** in $CDCl_3$ (162.00 MHz).

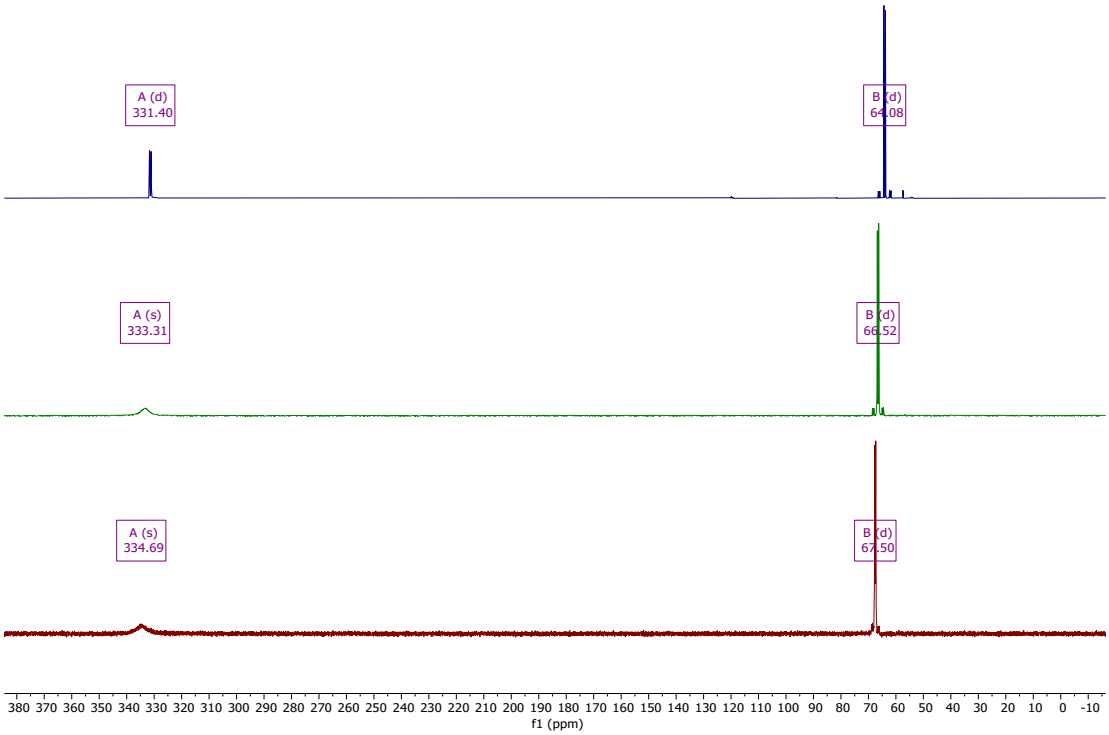

Figure S10b. Comparative analysis of $^{31}P\{H\}$ NMR spectra for the results of reaction of derivative **1** with $Au(SMe_2)Cl$ in a ratio of 1:1 (blue) and 1:2 respectively under the same reaction conditions (green, crude solution) and upon 8 hours of heating to the reflux temperature of the solvent (red crude solution).

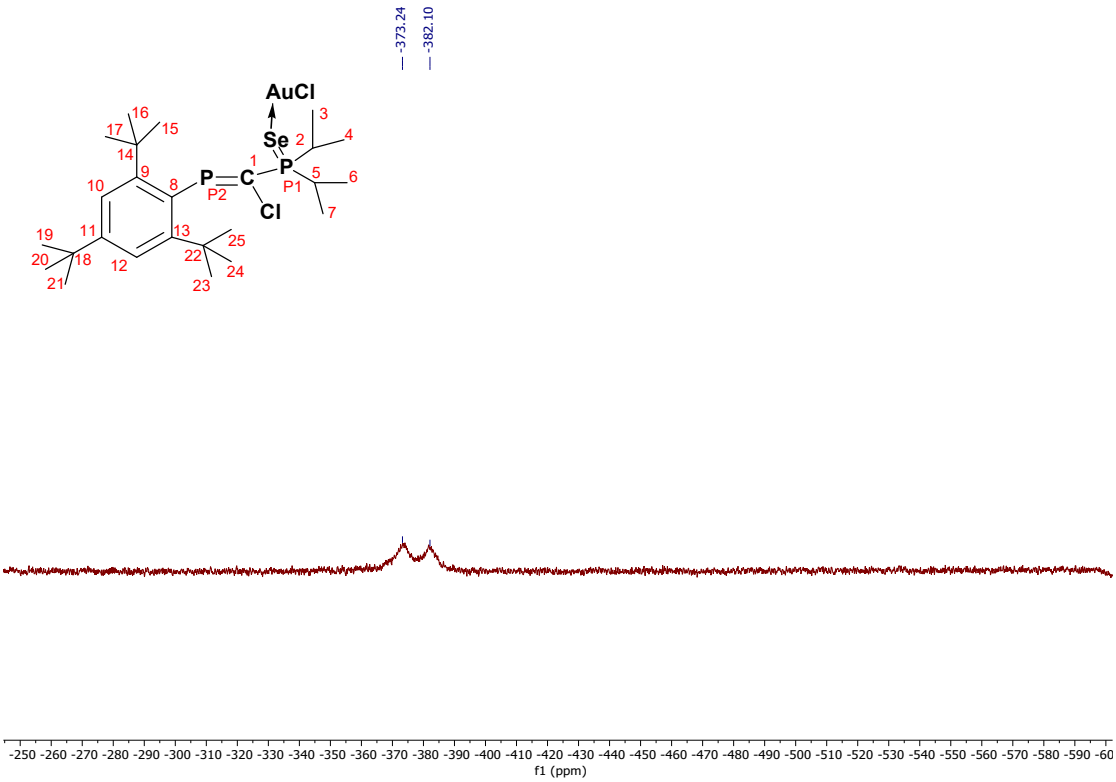

Figure S11. $^{77}Se\{H\}$ spectrum of **2** in $CDCl_3$ (76.31 MHz).

1.3. {Mes*P=C(Cl)-P(=Se)(*i*-Pr)$_2$}PdCl$_2$ **(3)**

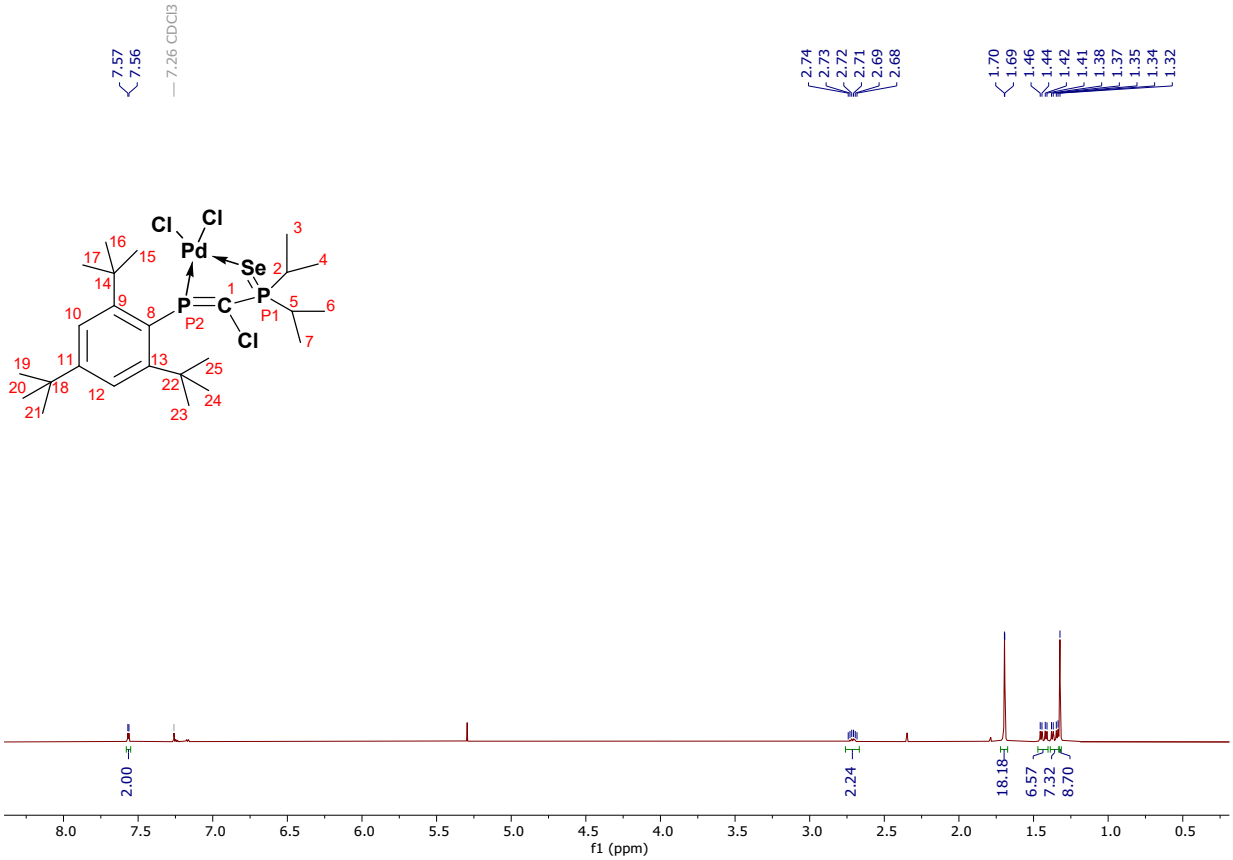

Figure S12. ^{1}H NMR spectrum of **3** in $CDCl_3$ (600.13 MHz).

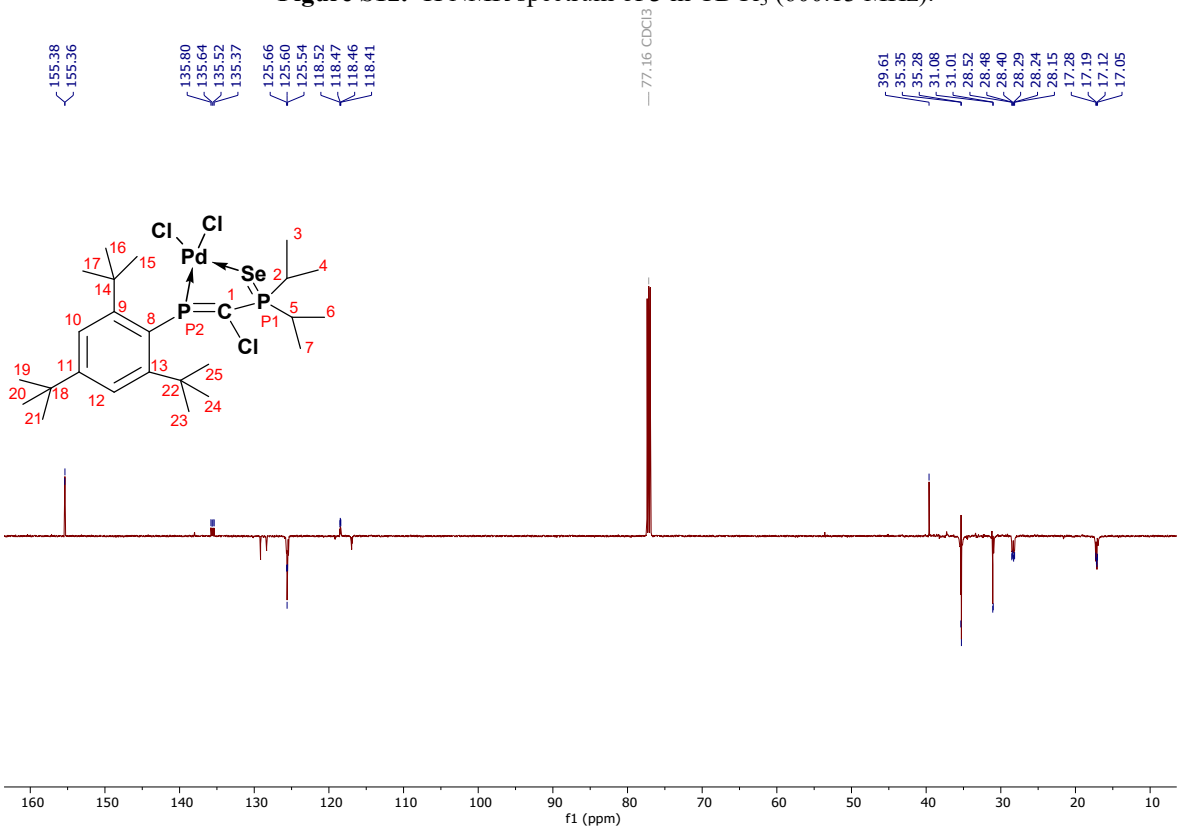

Figure S13. ^{13}C NMR spectrum of **3** in $CDCl_3$ (150.92 MHz).

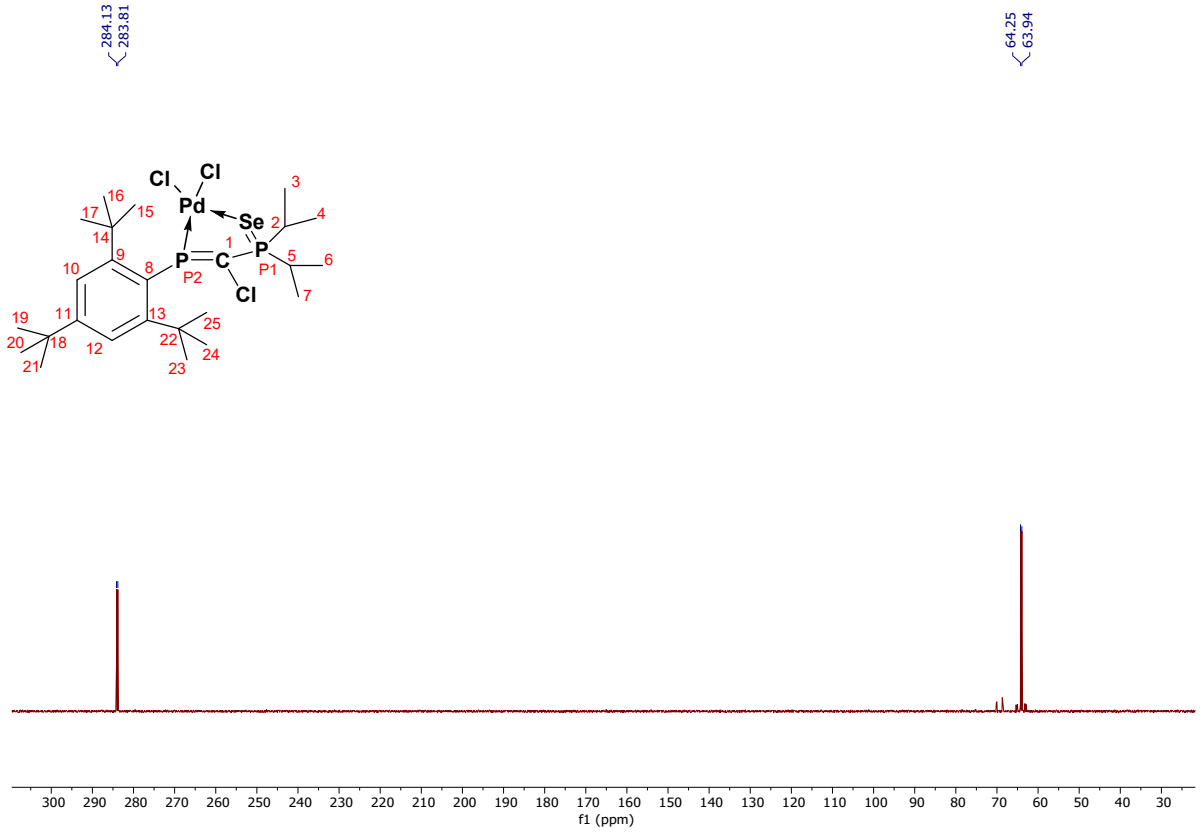

Figure S14. $^{31}P\{H\}$ NMR spectrum of **3** in $CDCl_3$ (242.97 MHz).

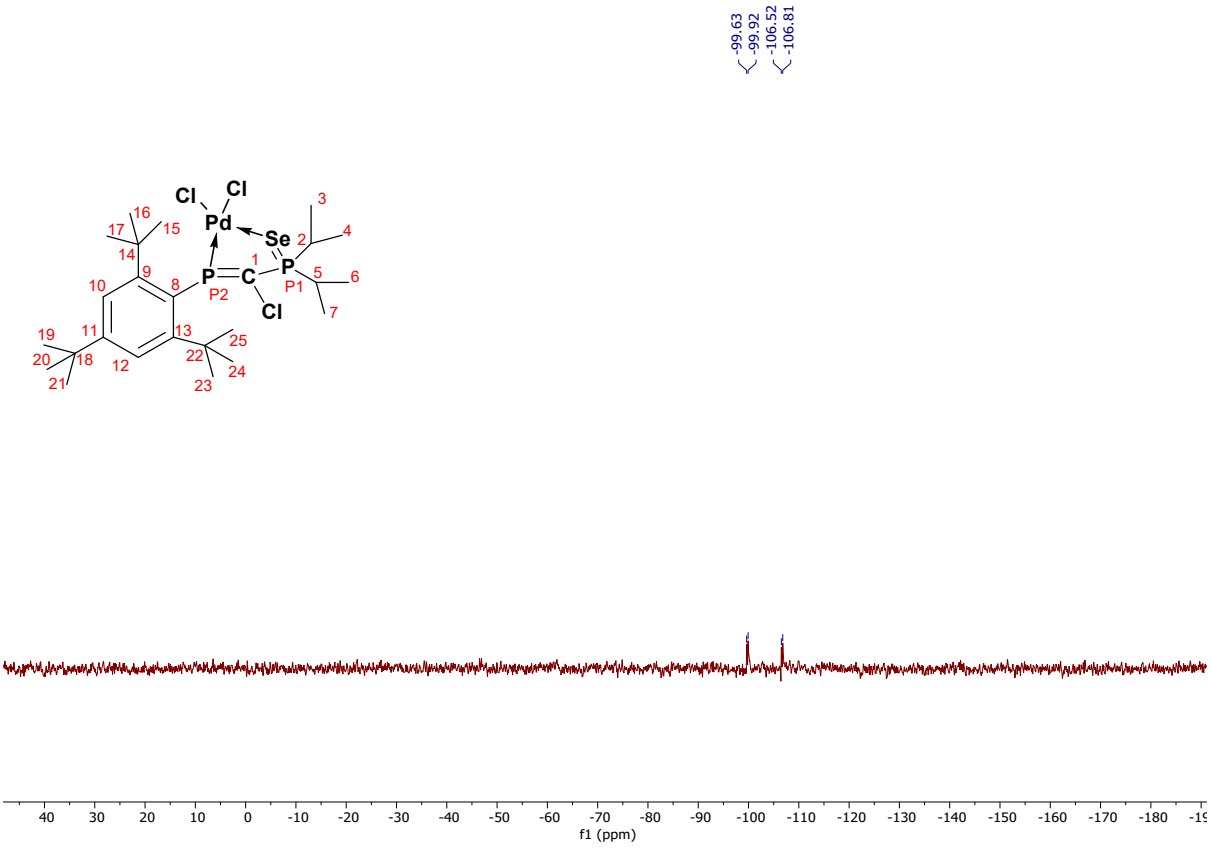

Figure S15. $^{77}Se\{H\}$ spectrum of **3** in $CDCl_3$ (76.31 MHz).

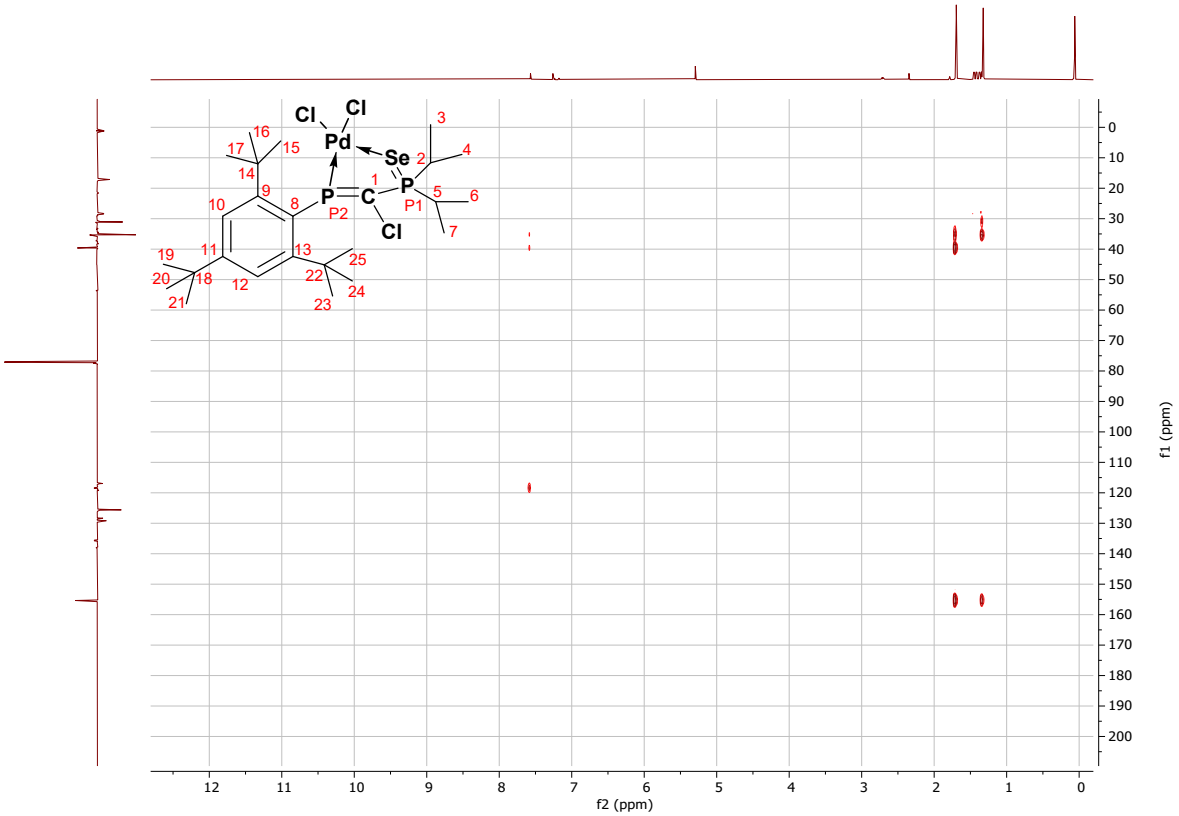

Figure S16. ^{1}H-^{13}C HMBC spectrum of **3** in $CDCl_3$ (600.13, 150.92MHz).

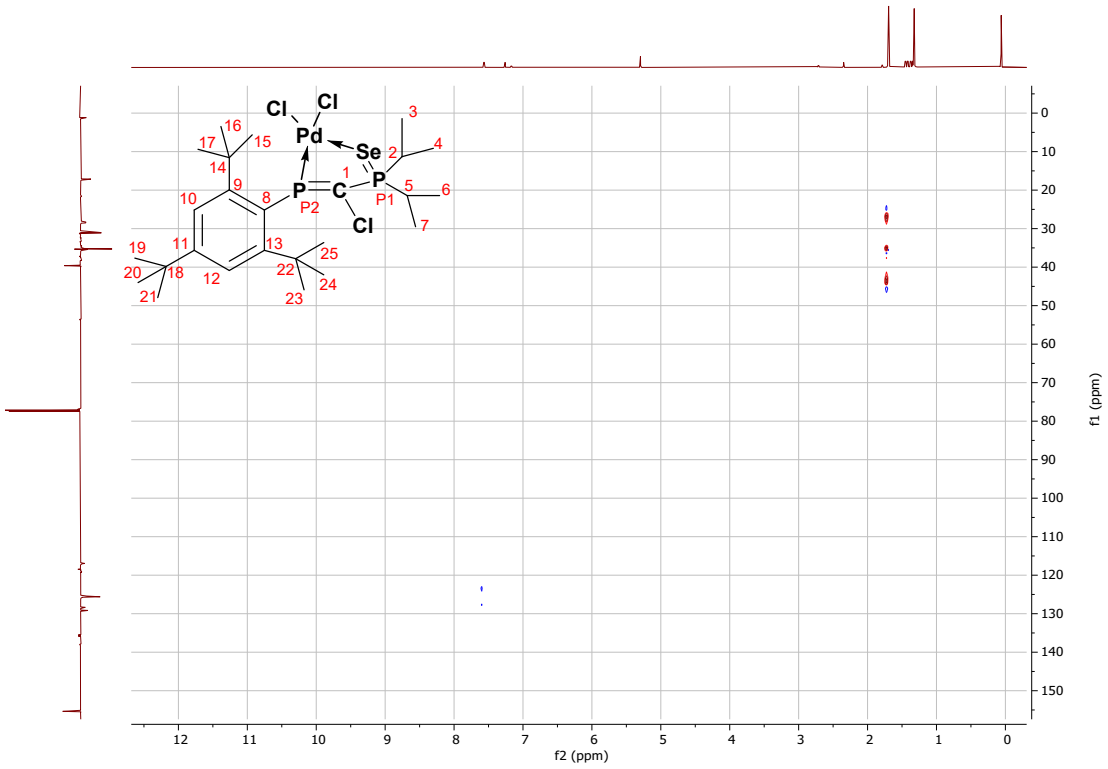

Figure S17. ^{1}H-^{13}C HSQC spectrum of **3** in $CDCl_3$ (600.13, 150.92MHz).

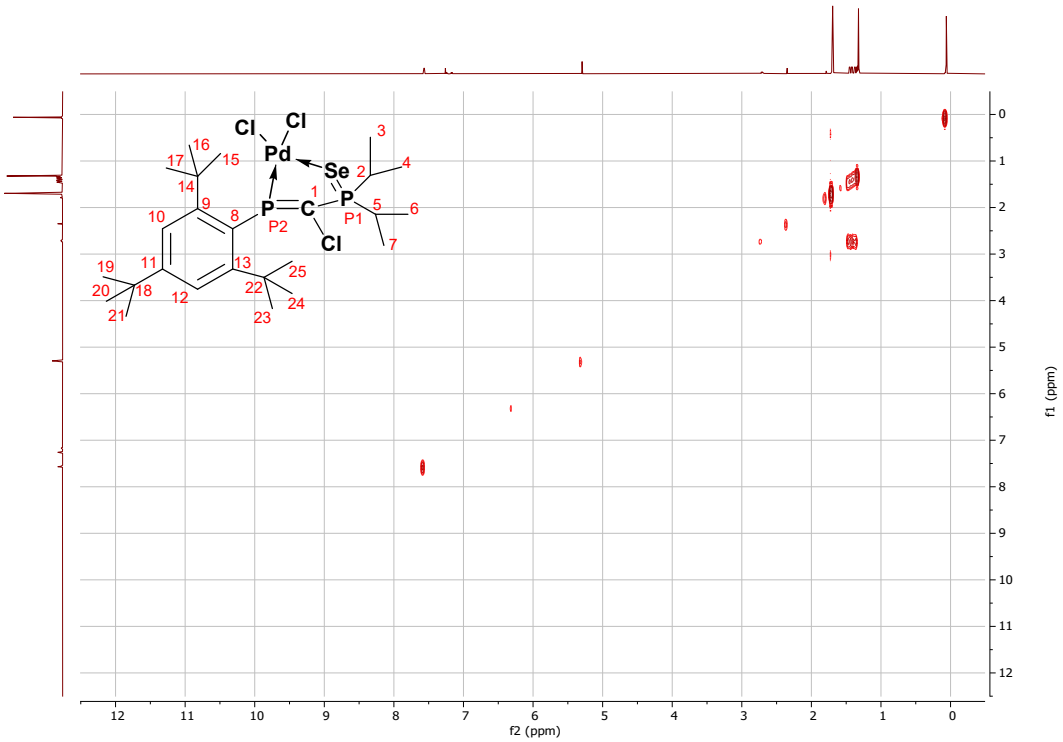

Figure S18. ^{1}H-^{1}H COSY spectrum of **3** in $CDCl_3$ (600.13, 600.13 MHz).

1.4. [{Mes*P=C(Cl)-P(=Se)(*i*-Pr)$_2$}Cu]$^{2+}$ **(4)**

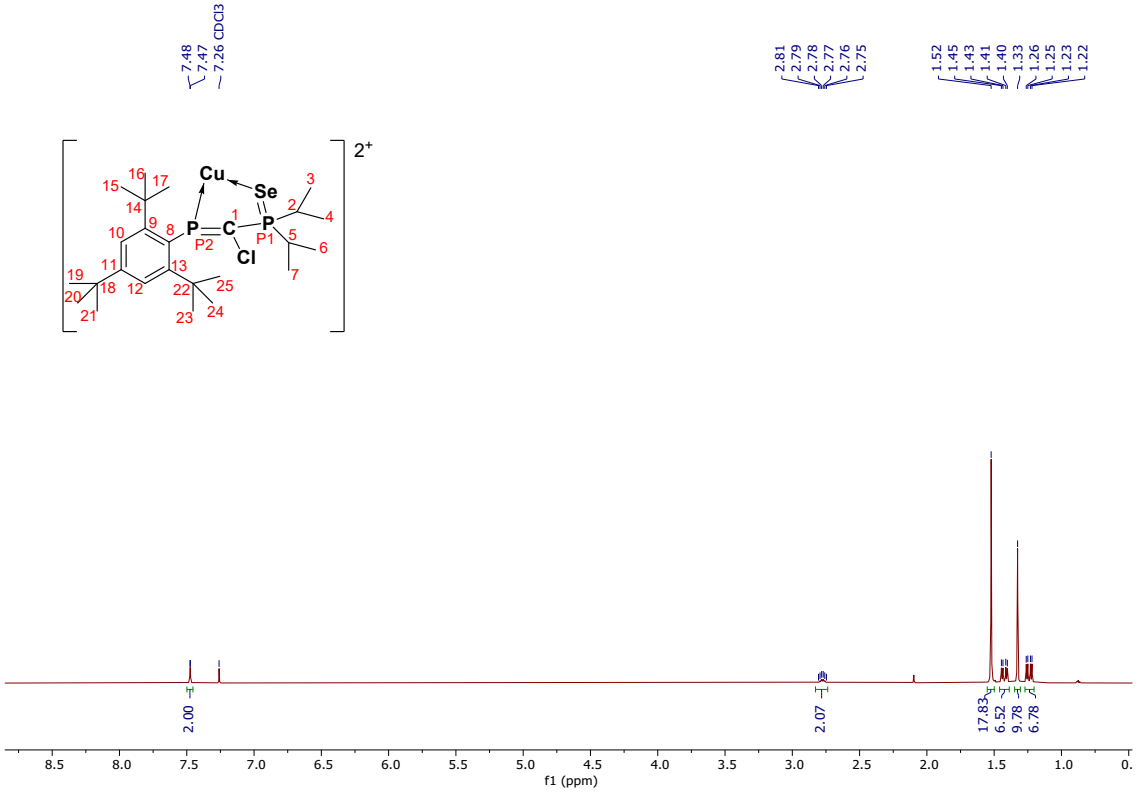

Figure S19. ^{1}H NMR spectrum of **4** in $CDCl_3$ (600.13 MHz).

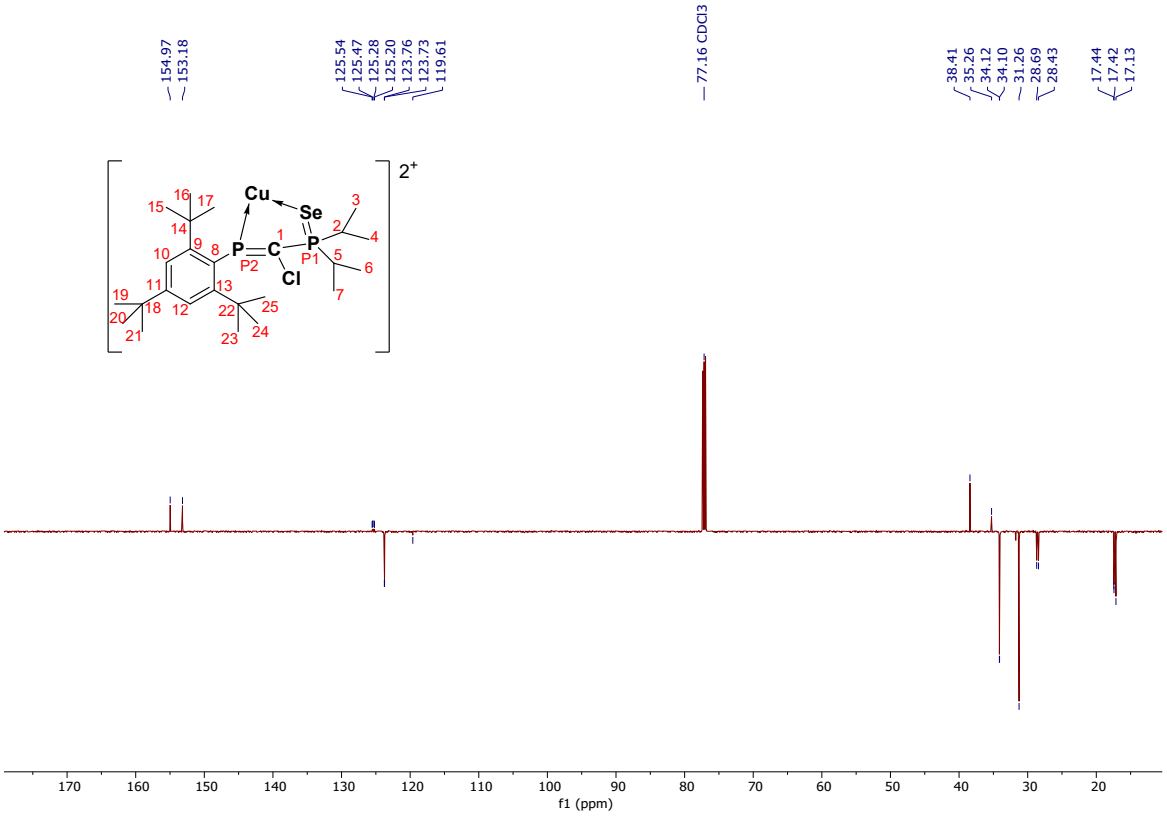

Figure S20. ^{13}C NMR spectrum of **4** in $CDCl_3$ (150.92 MHz).

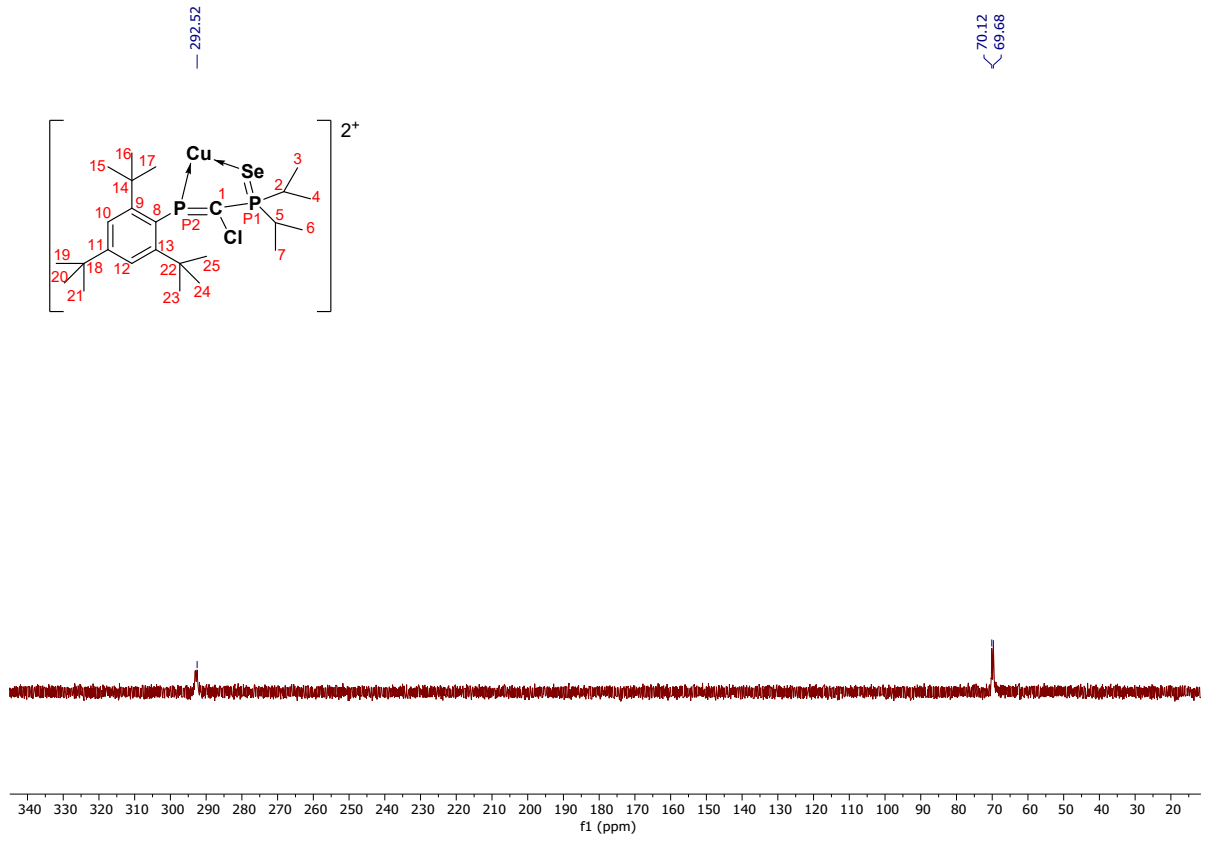

Figure S21. $^{31}P\{H\}$ NMR spectrum of **4** in $CDCl_3$ (242.97 MHz).

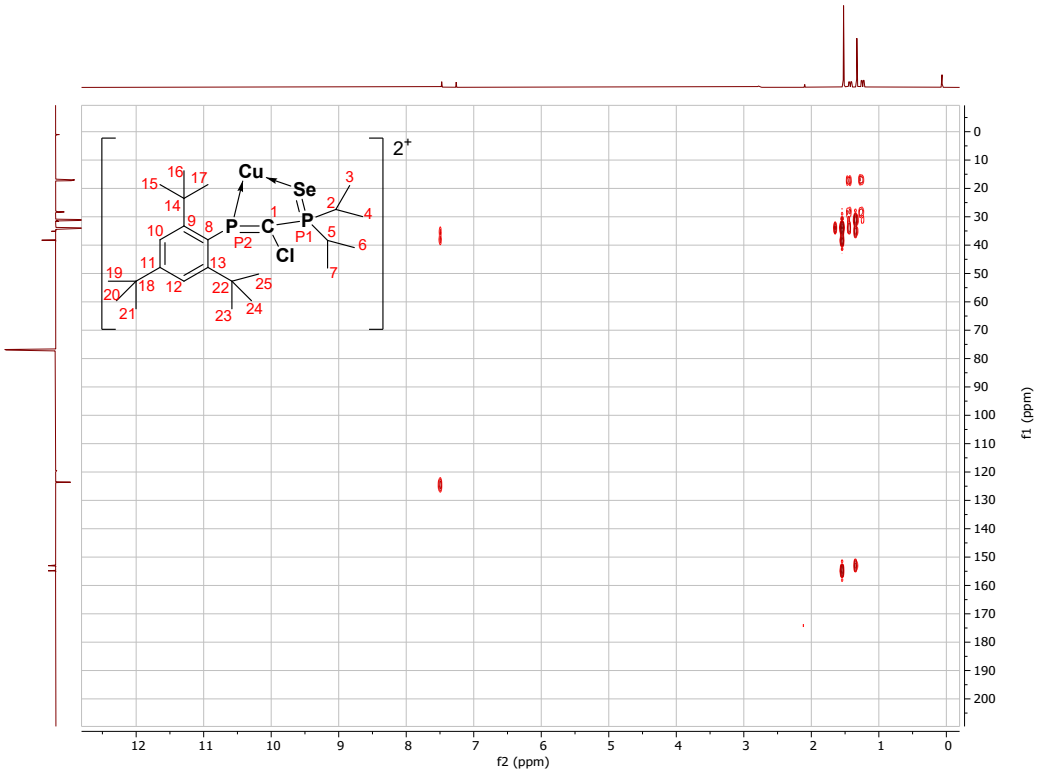

Figure S22. ^{1}H-^{13}C HMBC spectrum of **4** in $CDCl_3$ (600.13, 150.92MHz).

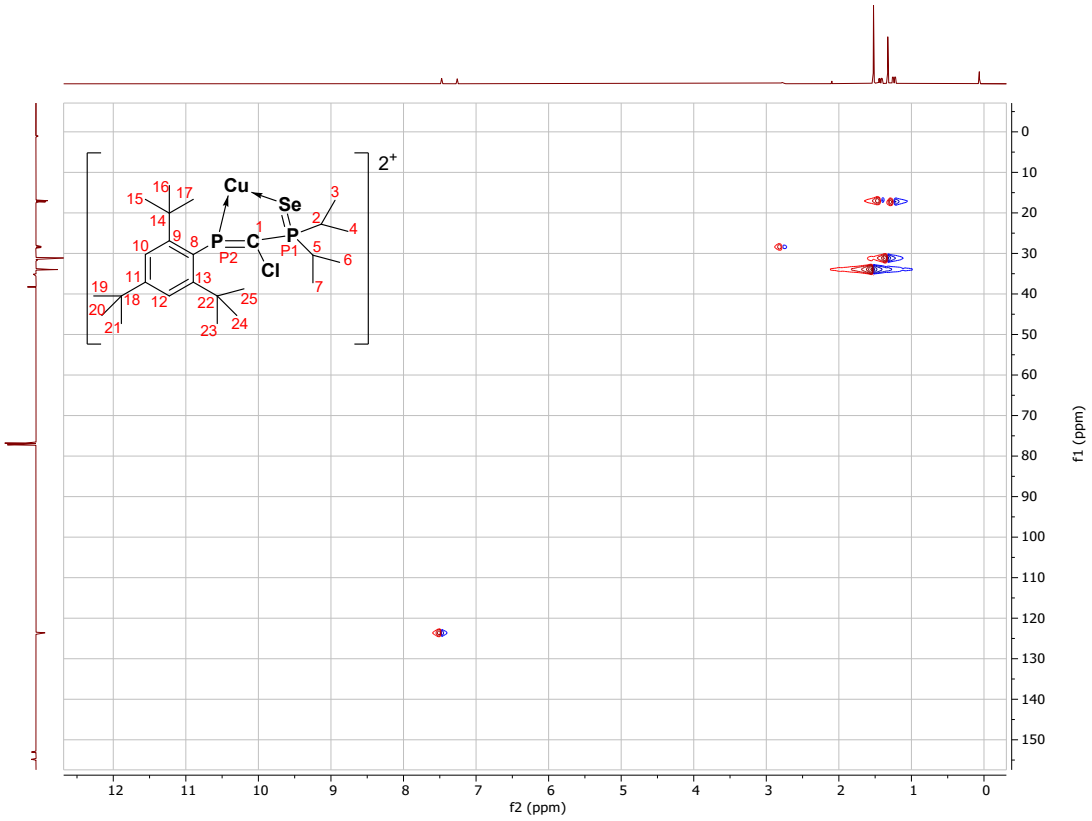

Figure S23. ^{1}H-^{13}C HSQC spectrum of **4** in $CDCl_3$ (600.13, 150.92MHz).

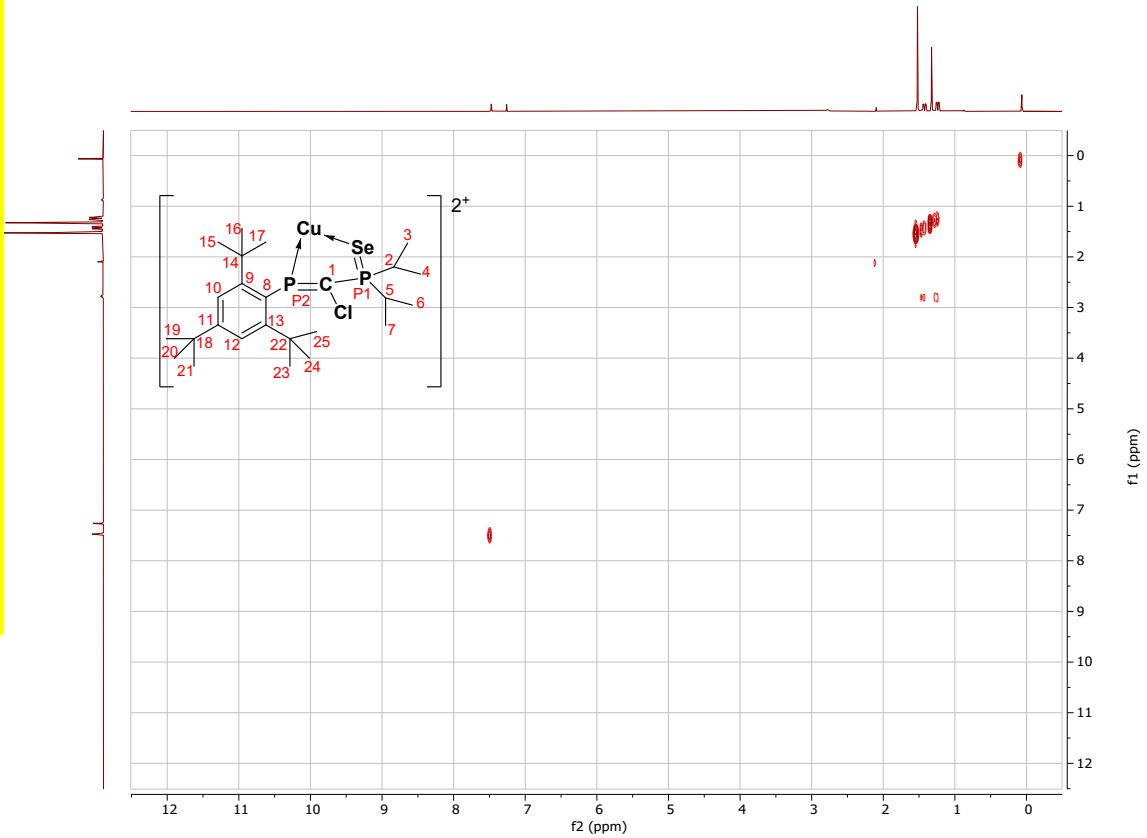

Figure S24. ^{1}H-^{1}H COSY spectrum of **4** in $CDCl_3$ (600.13, 600.13 MHz).

1.5. {[Mes*P=C(Cl)-P(=Se)(*i*-Pr)$_2$]$_2$}CuAu(Cl) **(5)**

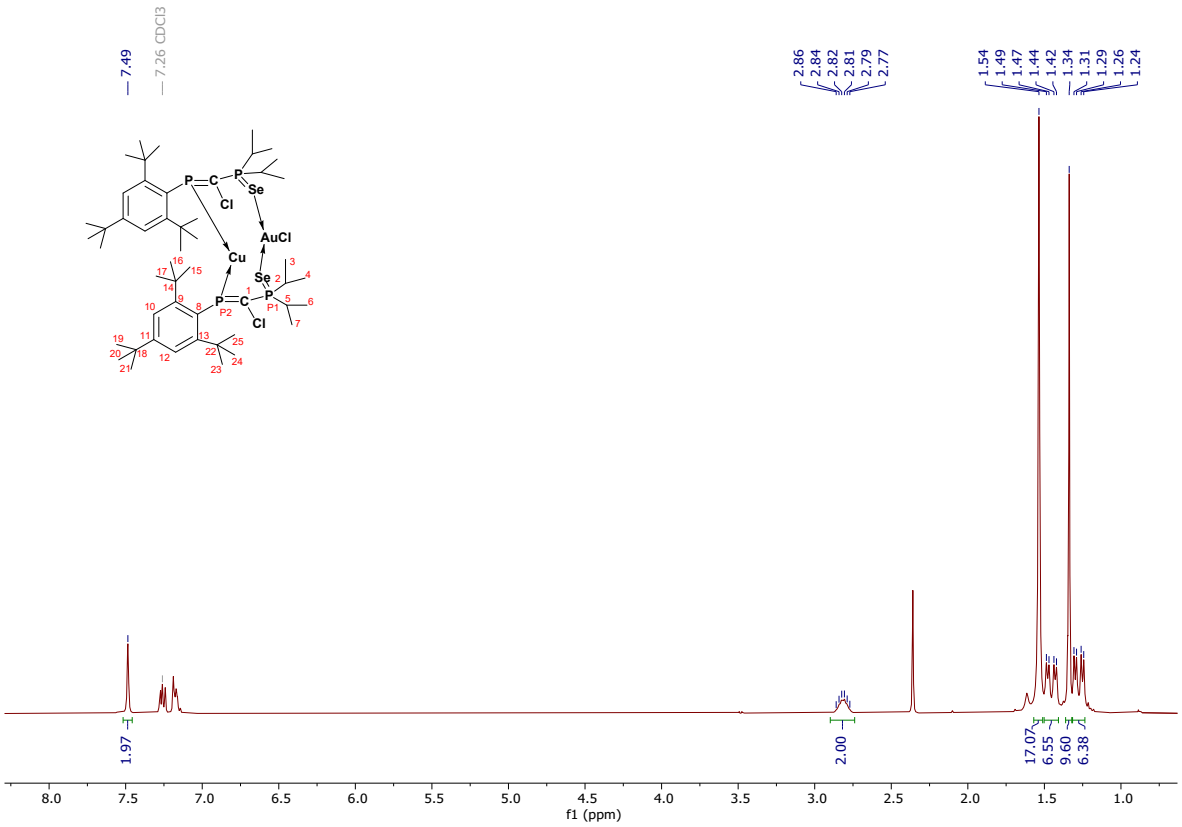

Figure S25. ^{1}H NMR spectrum of **5** in $CDCl_3$ (400.13).

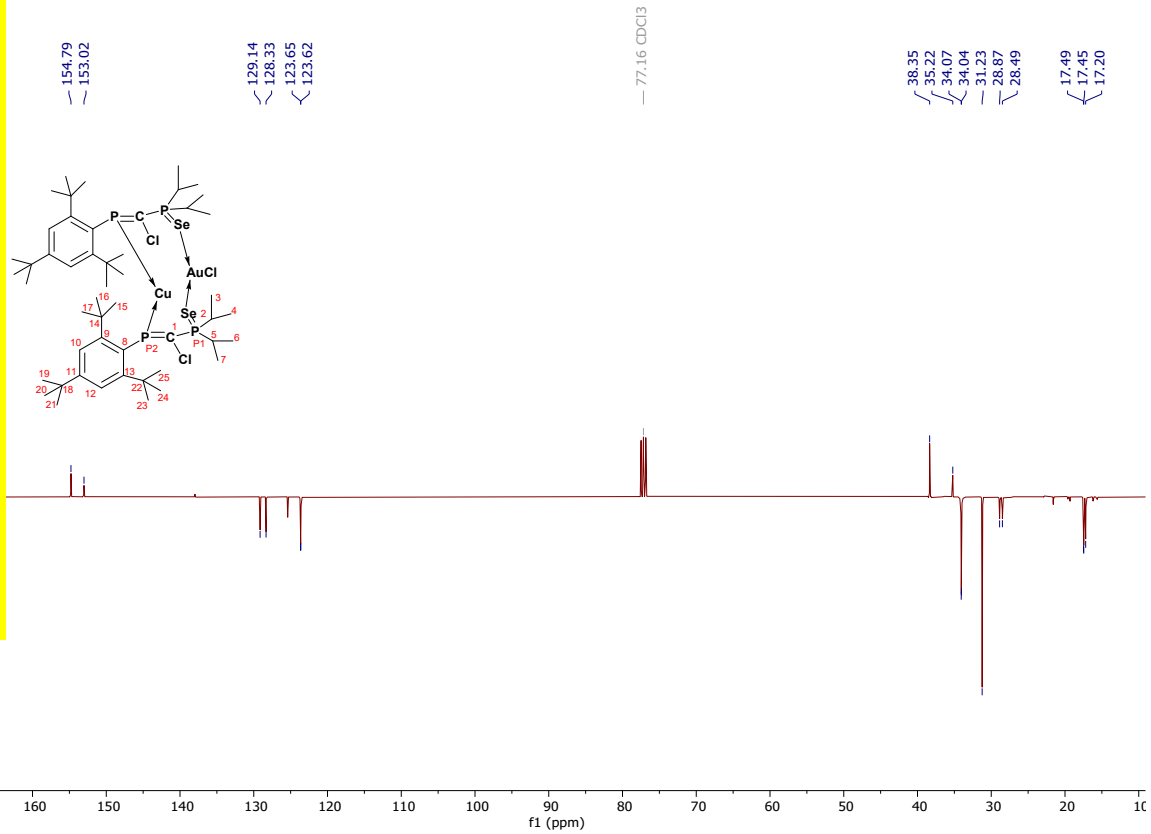

Figure S26. ^{13}C NMR spectrum of **5** in $CDCl_3$ (100.62 MHz).

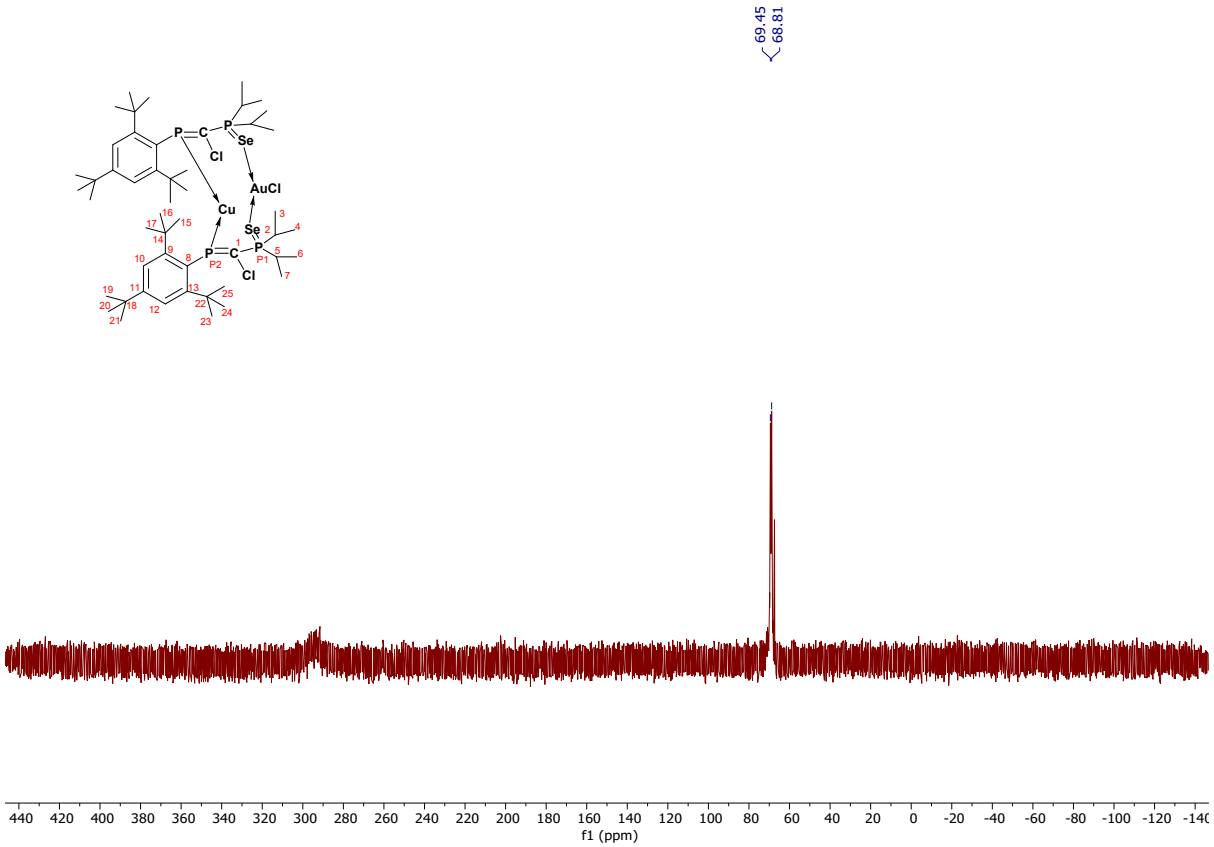

Figure S27. $^{31}P\{H\}$ NMR spectrum of **5** in $CDCl_3$ (162.00 MHz).

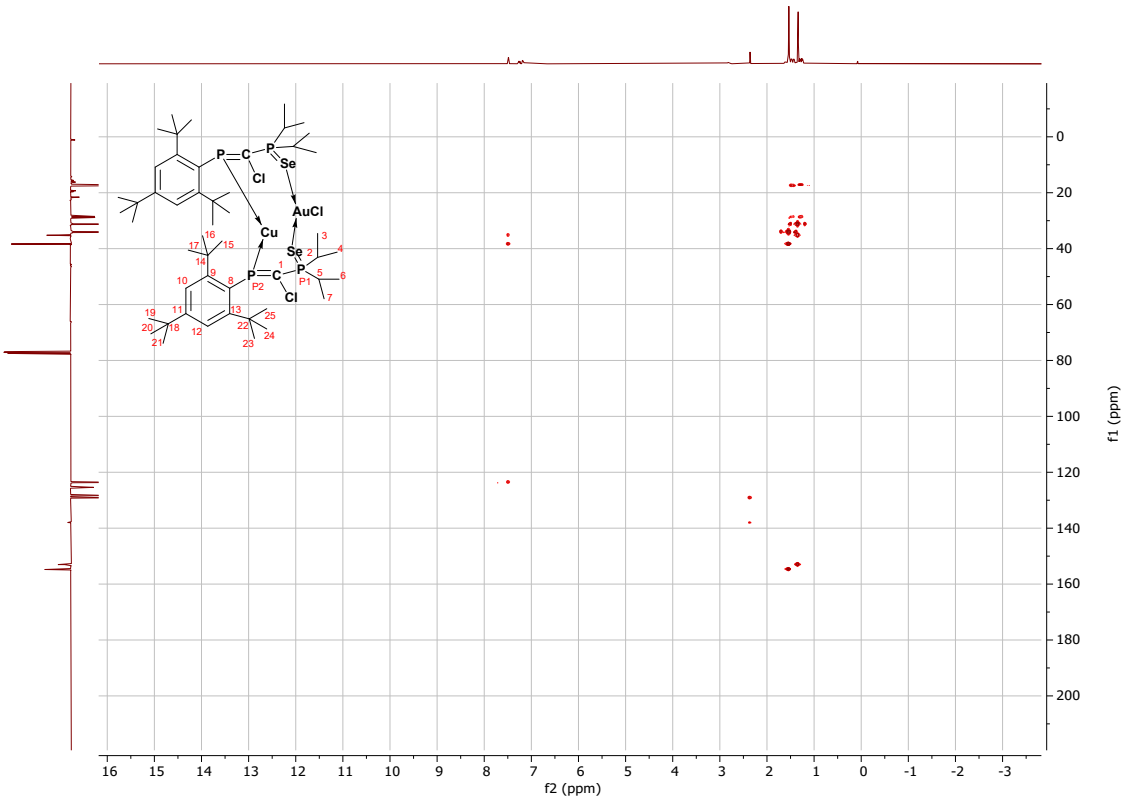

Figure S28. ^{1}H-^{13}C HMBC spectrum of **5** in $CDCl_3$ (400.13, 100.62MHz).

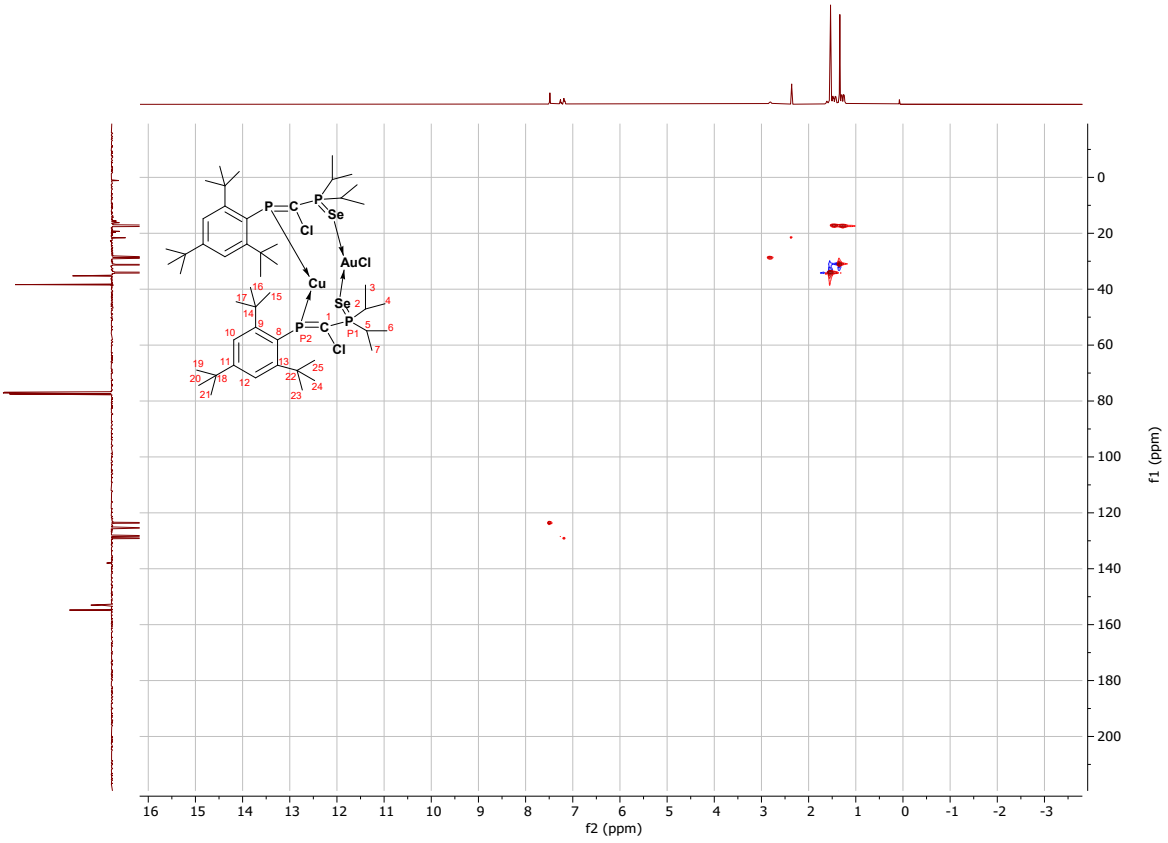

Figure S29. ^{1}H-^{13}C HSQC spectrum of **5** in $CDCl_3$ (400.13, 100.62MHz).

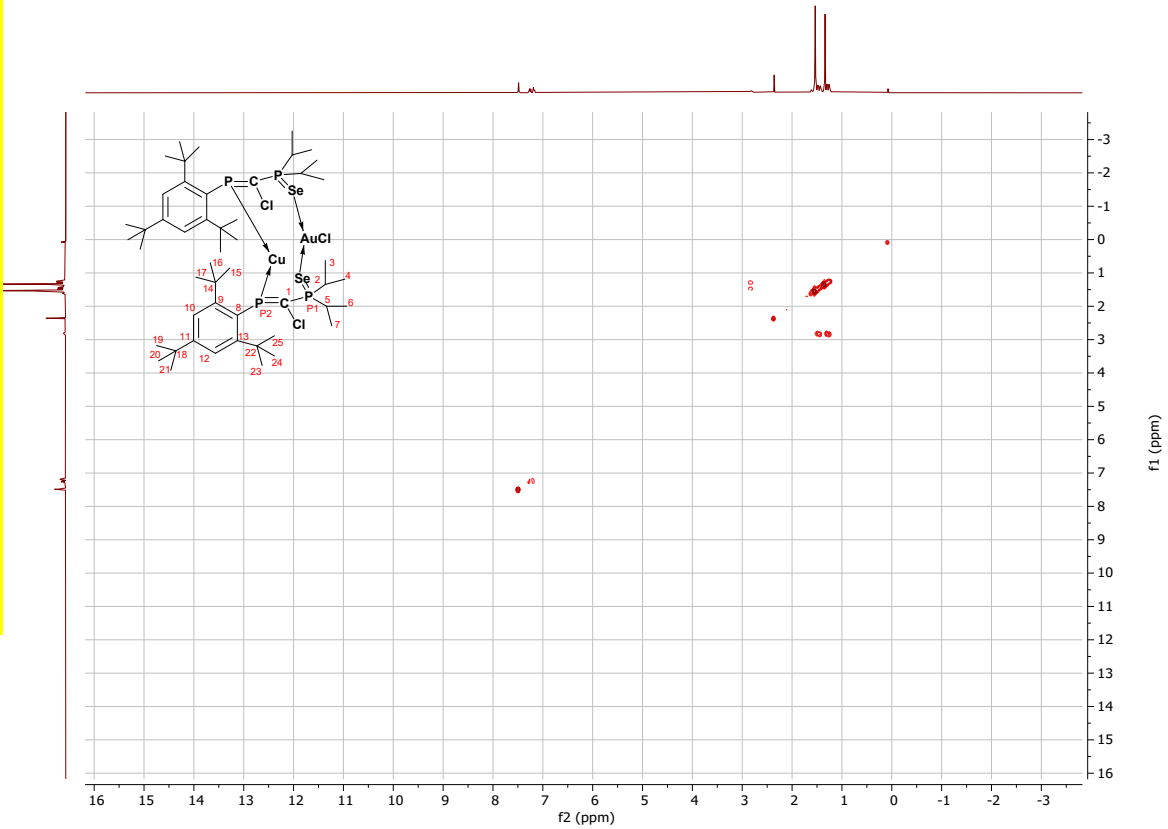

Figure S30. ^{1}H-^{1}H COSY spectrum of **5** in $CDCl_3$ (400.13, 400.13 MHz).

2. X-ray data

Table S1. Crystal data and refinement details for compounds **1** and **3**.

Compound	**1**	**3**·CH_2Cl_2
Molecular formula	$C_{25}H_{43}ClP_2Se$	$C_{25}H_{43}Cl_3P_2PdSe$, CH_2Cl_2
Formula weight	519.94	782.17
Crystal size / mm^3	0.160 x 0.064 x 0.060	0.132 x 0.131 x 0.106
Crystal habit	light yellow block	light orange plate
λ(MoK_α) / Å	0.71073	0.71073
T / K	100.(2)	100.(2)
Crystal system	monoclinic	orthorhombic
Space group	$P2_1/n$	$Pnma$
a / Å	6.6637(5)	9.6344(4)
b / Å	19.2509(12)	13.6183(7)
c / Å	22.2228(16)	25.1598(10)
α / °	90	90
β / °	95.852(2)	90
γ / °	90	90
V / Å^3	2835.9(3)	3301.1(3)
Z	4	4
D_{calc} / g cm^{-3}	1.218	1.574
μ / mm^{-1}	1.541	2.182
θ range for data collections (°)	2.12 - 28.28	2.26 - 27.88
F(000)	1096	1584
T_{max} / T_{min}	0.746 / 0.678	0.746/ 0.686
Refl. collected / unique / R_{int}	104006 / 7024 / 0.0455	176367 / 4100 / 0.0400
Completeness to θ	100%	100%
Refinement method	Full-matrix least-squares on F^2	Full-matrix least-squares on F^2
Data / restraints / parameters	7024 / 215 / 323	4100 / 0 / 189
Goodness-of-fit, S	1.037	1.079
Final R indices [$I>2\sigma(I)$]	R_1 = 0.0371	R_1 = 0.0231
	wR_2 = 0.0807	wR_2 = 0.0544
R indices (all data)	R_1 = 0.0452	R_1 = 0.0249
	wR_2 = 0.0855	wR_2 = 0.0557
$\Delta\rho_{max}$, $\Delta\rho_{min}$ / e Å^{-3}	1.650; -1.385	0.790; -0.769
CCDC No.	**2448919**	**2448920**

Table S2. Selected geometrical parameters for compound **1**.

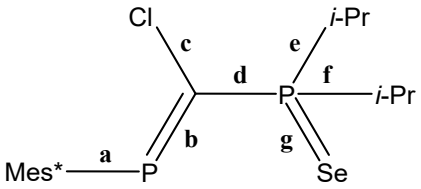

	bond length (Å)		**angles (°)**
a	1.849(2)	**b-d**	119.6(1)
b	1.680(2)	**b-c**	125.8(1)
c	1.746(2)	**c-d**	114.6(1)
d	1.820(2)	**d-e**	106.4(1)
e	1.835(2)	**e-f**	106.9(1)
f	1.838(2)	**e-g**	112.6(1)
g	2.110(1)	**d-f**	108.5(1)
		d-g	110.8(1)
		g-d-c	163.6(1)
		g-d-b	-15.2(1)

In compound **1** two of the *tert*-butyl groups in the 2,4,6-tri-*tert*-butylphenyl (Mes*) moiety were found to be disordered on two positions with a refined occupancy ratio of 80:20 for the *ortho* group and 60:40 for the *para* group respectively.

Compound **2** crystallizes as a solvate with one molecule of chloroform (Figure S19).

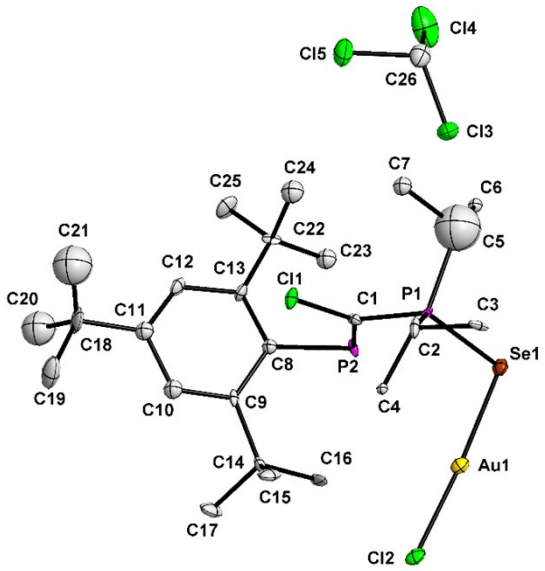

Figure S31. The asymmetric unit of **2** shown with 50% probability ellipsoids (except for some carbon atoms that have NPD ellipsoids and that are shown with isotropic thermal ellipsoids). Hydrogen atoms were not introduced in this partial model.

Table S3. Selected geometrical parameters for compound **2**.

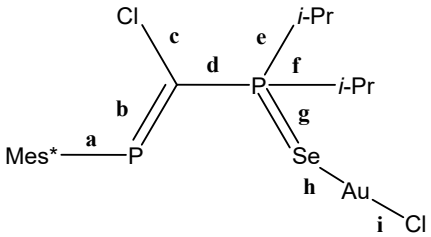

Bond length (Å)		Angles (°)	
a	1.86(3)	**b-c**	126.2(15)
b	1.69(3)	**b-d**	119.7(15)
c	1.73(3)	**c-d**	114.1(14)
d	1.82(3)	**d-e**	109.5(13)
e	1.84(3)	**d-g**	112.8(9)
g	2.188(7)	**e-g**	114.4(9)
h	2.376(3)	**g-h**	97.8(2)
i	2.290(7)	**h-i**	175.7(2)
		h-g-d	-67.9(1)
		g-d-c	160.4(1)
		g-d-b	-16(2)

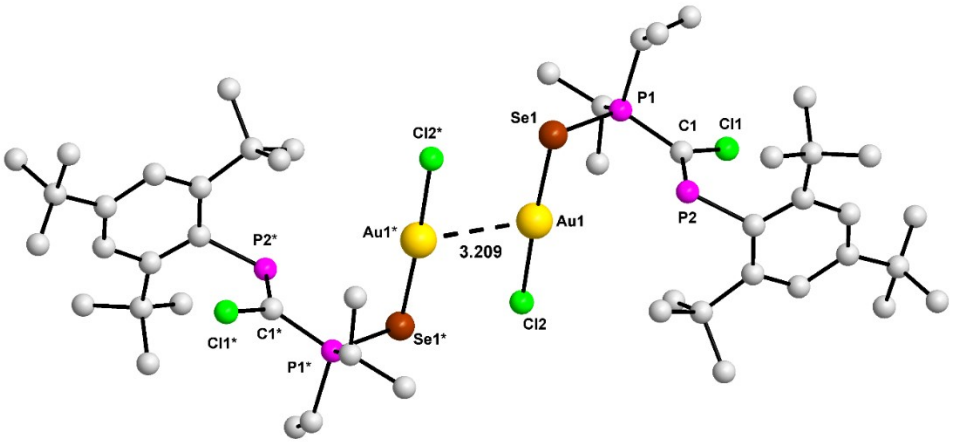

Figure S32. Dimeric unit established by Au···Au interaction in the crystal of **2**. Symmetry equivalent atoms are given by * (1-x, 1-y, 1-z).

In compound **3**, the organic ligand coordinates to palladium in a bidentate mode, through P2 and Se1 atoms. The geometry around the metal center is almost ideal square planar, with calculated geometry parameters indices $\tau_4 = 0.05$ [1] and $\tau_4' = 0.04$ [2,3] (see also data in Table S4).

Table S4. Selected geometrical parameters for compound **3**.

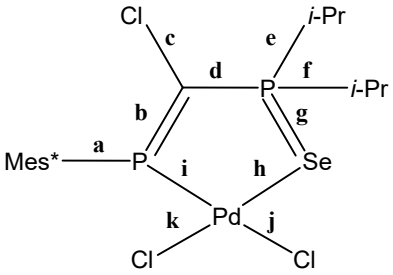

	Bond length (Å)		Angles (°)
a	1.817(2)	**b-c**	127.3(2)
b	1.670(3)	**b-d**	118.6(2)
c	1.726(3)	**c-d**	114.1(2)
d	1.796(3)	**d-e**	107.8(1)
e	1.834(3)	**e-f***	110.1(1)
f*	1.834(3)	**e-g**	111.8(1)
g	2.176(1)	**d-f***	107.8(1)
h	2.398(1)	**h-i**	91.6(1)
i	2.203(1)	**i-j**	176.3(1)
j	2.341(1)	**i-k**	91.2(1)
k	2.307(1)	**j-k**	92.5(1)
		h-j	84.7(1)
		h-k	177.2(1)

*Involves symmetry (x, 1/2-y, z) generated *i*-Pr group

3. HRMS analysis of compound **(5)**

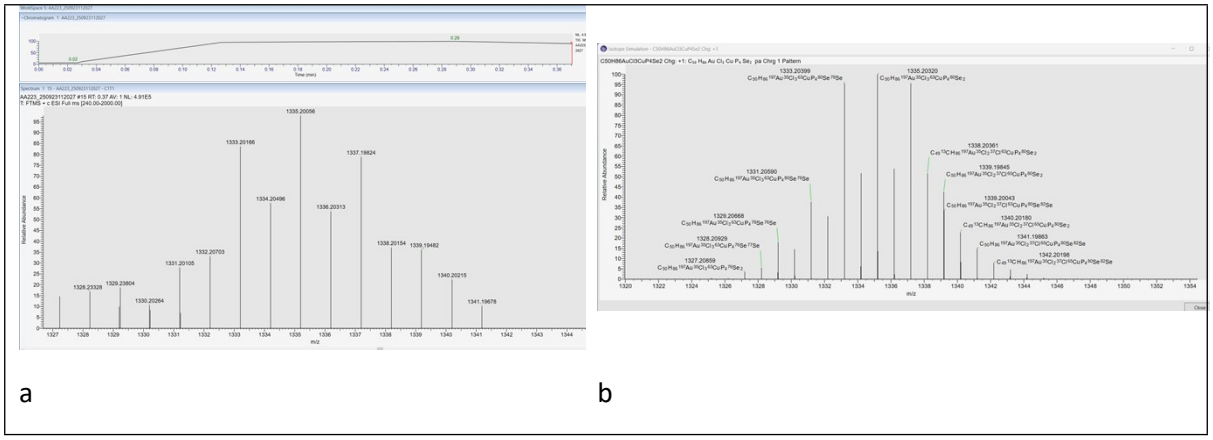

Figure S33. HRMS spectra (ESI) showing the molecular peak of compound **5**, $C_{50}H_{86}AuCl_3CuP_4Se_2$ (a) versus its simulated isotope distribution (b).

4. Theoretical investigations: DFT calculations and UBDE, EDA, NBO analyses

4.1. Computational results

Computational analyses were performed on Mes*P=C(Cl)-P(=X)(*i*-Pr)$_2$ (X = O, S, Se) systems, to understand their structural and electronic properties, and their coordination preferences to gold and palladium centers. Thus, the thermal stability of model {Mes*P=C(Cl)-P(=X)(*i*-Pr)$_2$}AuCl and {Mes*P=C(Cl)-P(=X)(*i*-Pr)$_2$}PdCl$_2$ complexes were evaluated, as well as the energy difference between possible coordination isomers obtained through X→M (X = O, S, Se) and P(III)→M bonds (M = Au or Pd). Data derived from theoretical explorations and related discussions are presented below, grouped into dedicated subsections for each class of the model derivatives investigated herein.

4.1.1. Mes*P=C(Cl)-P(=X)(*i*-Pr)$_2$ systems (X = O, S, Se)

DFT calculations were carried out to assess the electronic-structure of targeted selenium-based Mes*P=C(Cl)-P(=**Se**)(*i*-Pr)$_2$ complex (**1** in the main text). The initial geometry of **1** was imported from X-ray data.

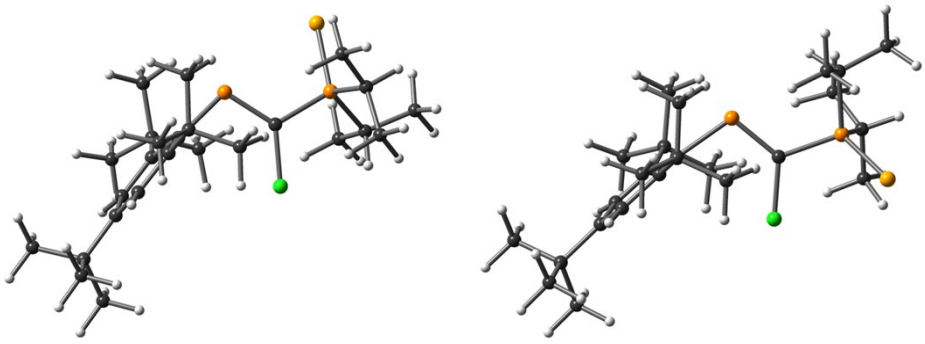

Figure S34. Equilibrium geometries of the conformers investigated in the DFT study. *Left* – conformation which closely resembles the solid-state structure (*conformer 1 cis*). *Right* – conformation obtained through the rotation with 180º with respect to the C-P(sp^3) σ-bond (*conformer 2 trans*).

An in-depth theoretical investigation of an extended series of phosphavinyl(calcogenoxo)phosphorane derivatives should allow a better understanding of the electronic features within the P=C-P(=X) backbone (X = chalcogen atom) and could play a crucial in the rational design of novel complexes stabilized by this electron-rich unit. The goal is to understand whether the type of X chalcogen atom could impact the stability and/or selectivity of targeted compounds.

Table S5. Relative energies for the investigated conformers of Mes*P=C(Cl)-P(=X)(*i*-Pr)$_2$ (X = O, S, Se) systems.

X	O	S	Se
Conformation	relative ΔG° values (kcal mol^{-1})		
conformer 1	0.0	0.0	0.0
conformer 2	2.5	2.6	2.6

Table S6. Natural bond orders computed for the atoms contained in the P=C-P(=X) (X = O, S, Se) unit of the Mes*P=C(Cl)-P(=X)(*i*-Pr)$_2$ derivatives, in the two investigated conformations.

Bond Order	P=C-P(=O)			P=C-P(=S)			P=C-P(=Se)		
	P=C	C-P	P=O	P=C	C-P	P=S	P=C	C-P	P=Se
					conformer 1				
total	1.86	0.82	**1.49**	1.86	0.82	**1.50**	1.86	0.85	**1.45**
covalent	1.32	0.56	0.62	1.29	0.60	1.08	1.29	0.61	1.05
ionic	0.54	0.26	0.87	0.56	0.22	0.41	0.57	0.23	0.40
					conformer 2				
total	1.84	0.79	**1.50**	1.84	0.78	**1.55**	1.84	0.80	**1.52**
covalent	1.36	0.54	0.63	1.35	0.56	1.11	1.34	0.58	1.12
ionic	0.49	0.25	0.88	0.50	0.21	0.44	0.50	0.22	0.39

4.1.2. {Mes*P=C(Cl)-P(=X)(*i*-Pr)$_2$}AuCl complexes (X = O, S, Se)

DFT calculations, coupled with several other computational techniques (unrelaxed bond dissociation energy (UBDE), energy decomposition analysis (EDA) and NBO calculations), were conducted on the series of {Mes*P=C(Cl)-P(=X)(*i*-Pr)$_2$}AuCl (X= O, S and Se), to better understand their electronic features, especially their coordination preferences. In this respect, the relative stability of complexes obtained through P(III)→Au (Figure S23 – *left*) and X→Au (Figure S23 – *right*) donations were assessed (see discussions in the *main text*), both in gaseous phase (Table S8) and dichloromethane (Table S9). For the calculations carried out in DCM, a polarizable continuum model (PCM) was employed (further details about the PCM model employed are presented in the *Computational Details* section).

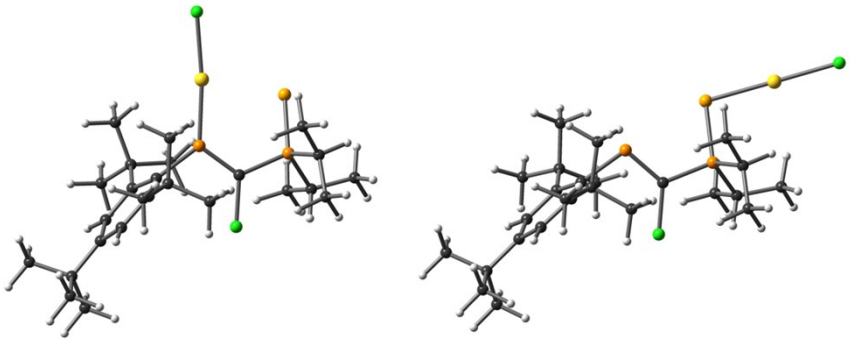

Figure S35. Equilibrium geometries of model {Mes*P=C(Cl)-P(=X)(*i*-Pr)$_2$}AuCl (X= O, S and Se) complexes formed via P(III)→Au (*left*) and X→Au (*right*) bonds.

Table S7. Relative stability between molecular {Mes*P=C(Cl)-P(=X)(*i*-Pr)$_2$}AuCl complexes formed via P(III)→Au and X→Au bonds (X= O, S and Se), according to the DFT calculations performed in gaseous phase.

{Mes*P=C(Cl)-P(=X)(*i*-Pr)$_2$}AuCl	**P(III)→Au**	**X→Au**
	relative ΔG° values (kcal mol^{-1})	
X = O	0.0	10.6
X = S	1.2	0.0
X = Se	2.5	0.0

Table S8. Relative stability between molecular {Mes*P=C(Cl)-P(=X)(*i*-Pr)$_2$}AuCl complexes formed via P(III)→Au and X→Au bonds (X= O, S and Se), according to the DFT calculations performed in DCM.

{Mes*P=C(Cl)-P(=X)(*i*-Pr)$_2$}AuCl	**P(III)→Au**	**X→Au**
	relative ΔG° values (kcal mol^{-1})	
X = O	0.0	12.8
X = S	0.4	0.0
X = Se	2.6	0.0

UBDE and EDA calculations were carried out on the optimized molecular geometries of {Mes*P=C(Cl)-P(=X)(*i*-Pr)$_2$}AuCl complexes, to gain more insight into the strength and nature of the P(III)→Au and X→Au bonds. The UBDE values are presented in Table e in the *main text*, while the EDA schemes in Table S9. Further discussions regarding these data are presented in the *main text.*

Table S9. Calculated EDA decomposition schemes for {Mes*P=C(Cl)-P(=X)(*i*-Pr)$_2$}AuCl complexes formed via P(III)→Au or X→Au bonds (X= O, S and Se). All energy values are reported in *kcal mol^{-1}*.

Decomp. Scheme	Total Energy Interaction	Electrost. Interaction	Exchange-Repulsion	Exchange Interaction	Repulsion	Orbital Relaxation	Total Stabilization	% Electrostatic	% Covalent
*{Mes*P=C(Cl)-P(=**O**)(i-Pr)$_2$}AuCl model complexes*									
O→Au	**-42.11**	-55.00	73.27	-38.74	112.01	-47.23	-102.23	53.80	46.20
P(III)→Au	**-54.60**	-66.60	131.55	-74.09	205.64	-97.28	-163.88	40.64	59.36
*{Mes*P=C(Cl)-P(=**S**)(i-Pr)$_2$}AuCl model complexes*									
S→Au	**-53.91**	-65.47	105.93	-60.54	166.47	-75.39	-140.86	46.48	53.52
P(III)→Au	**-54.25**	-70.36	139.46	-78.80	218.26	-99.11	-169.47	41.52	58.48
*{Mes*P=C(Cl)-P(=**Se**)(i-Pr)$_2$}AuCl model complexes*									
Se→Au	**-54.91**	-63.44	101.04	-59.62	160.66	-73.81	-137.25	46.22	53.78
P(III)→Au	**-54.41**	-72.90	144.20	-81.56	225.76	-100.54	-173.44	42.03	57.97

Table S10. Natural charges computed for the atoms contained in the P=C-P(=X)-Au backbone, for the {Mes*P=C(Cl)-P(=X)(*i*-Pr)$_2$}AuCl complexes involving either P(III)→Au or X→Au bonds (X= O, S and Se).

P=C-P(=X)-Au backbone	P(III)	C	P(V)	X	Au
formed via X→Au donations					
X = O	0.840	-0.925	1.961	-1.114	0.424
X = S	0.834	-0.915	1.394	-0.497	0.336
X = Se	0.832	-0.918	1.300	-0.370	0.308
formed via P(III)→Au donations					
X = O	0.825	-0.899	1.946	-1.102	0.437
X = S	0.832	-0.894	1.354	-0.591	0.442
X = Se	0.833	-0.903	1.256	-0.493	0.446

Table S11. Natural bond orders computed for the atoms within the P=C-P(=X)-Au backbone, for the {Mes*P=C(Cl)-P(=X)(*i*-Pr)$_2$}AuCl complexes involving either P(III)→Au or X→Au bonds (X= O, S and Se).

Bond Order	P=C-P(=O)				P=C-P(=S)				P=C-P(=Se)			
	P=C	**C-P**	**P=O**	**X→Au**	**P=C**	**C-P**	**P=S**	**X→Au**	**P=C**	**C-P**	**P=Se**	**X→Au**
	formed via X→Au donations											
total	1.89	0.93	1.13	**0.27**	1.89	0.99	1.04	**0.47**	1.90	1.01	1.15	**0.50**
covalent	1.30	0.66	0.45	0.06	1.29	0.71	0.93	0.20	1.29	0.72	0.98	0.23
ionic	0.60	0.27	0.68	0.21	0.61	0.27	0.11	0.27	0.61	0.28	0.16	0.27
Bond Order	**P=C**	**C-P**	**P=O**	**P(III)→Au**	**P=C**	**C-P**	**P=S**	**P(III)→Au**	**P=C**	**C-P**	**P=Se**	**P(III)→Au**
	formed via P(III)→Au donations											
total	1.91	0.91	1.25	**0.51**	1.93	0.92	1.29	**0.50**	1.91	0.93	1.25	**0.51**
covalent	1.44	0.60	0.57	0.21	1.43	0.65	1.05	0.21	1.40	0.65	0.98	0.20
ionic	0.47	0.31	0.68	0.30	0.50	0.27	0.23	0.29	0.50	0.27	0.27	0.30

4.1.3. {Mes*P=C(Cl)-P(=X)(*i*-Pr)$_2$}PdCl$_2$ complexes (X = O, S, Se)

The series of {Mes*P=C(Cl)-P(=X)(*i*-Pr)$_2$}PdCl$_2$ (X= O, S, Se) complexes was investigated by theoretical means, to gain insight into their electronic structure and to evaluate the strength of P(III)→Pd and X→Pd donations.

The Mes*P=C(Cl)-P(=X)(*i*-Pr)$_2$ + Pd(COD)Cl$_2$ ⇌ {Mes*P=C(Cl)-P(=X)(*i*-Pr)$_2$}PdCl$_2$ + COD reaction was theoretically assessed in DCM (*i.e.*, DFT-PCM solvation model), in order to understand whether the formation of {Mes*P=C(Cl)-P(=X)(*i*-Pr)$_2$}PdCl$_2$ complexes is thermodynamically accessible (Table S12). Thus, it is shown that the formation of targeted chelate complexes is spontaneous only for X = S or Se, with the selenium-based complex being the most stable one (based on the computed $\Delta_r G^o$ values) within the investigated series.

Table S12. Calculated $\Delta_r G^o$ values for the Mes*P=C(Cl)-P(=X)(*i*-Pr)$_2$ + Pd(COD)Cl$_2$ ⇌ {Mes*P=C(Cl)-P(=X)(*i*-Pr)$_2$}PdCl$_2$ + COD reaction, in DCM.

X	$\Delta_r G^o$ (kcal mol^{-1})
O	3.1
S	-4.4
Se	-6.8

UBDE and NBO analyses were performed on the optimized molecular geometries of {Mes*P=C(Cl)-P(=X)(*i*-Pr)$_2$}PdCl$_2$ complexes (X = O, S, Se), to evaluate the strength and nature of the P(III)→Pd and X→Pd bonds. The computed UBDE values are presented in Table S13. However, unlike the case of gold complexes, where the study of coordinate bond strengths was straightforward due to a monodentate binding fashion of both P(III)→Au and X→Au bonds, for the palladium complexes the computed UBDE values correspond to a cumulative effect of both P(III)→Pd and X→Pd donations (because the PdCl$_2$ fragment forms chelate complexes with the P=C-P(=X) unit). However, given that the interaction-energy of P(III)→Pd donation is expected to be constant in all of the {Mes*P=C(Cl)-P(=X)(*i*-Pr)$_2$}PdCl$_2$ (X = O, S, Se) complexes (*i.e.*, see for comparison Table S9 in which the computed UBDE values for the P(III)→Au bonds of investigated gold complexes are 54.5±0.2 kcal mol^{-1}, regardless of the X chalcogen atom), it is suggested that the X→Pd bond strength increases with *ca.* 11 kcal mol^{-1} from O to S, and with *ca.* 3.5 kcal mol^{-1} from S to Se.

Table S13. Calculated UBDE values for {Mes*P=C(Cl)-P(=X)(*i*-Pr)$_2$}PdCl$_2$ (X= O, S and Se) complexes.

X	UBDE value (kcal mol^{-1})
O	70.9
S	81.7
Se	84.9

NBO calculations were performed on the entire series of {Mes*P=C(Cl)-P(=X)(*i*-Pr)$_2$}PdCl$_2$, to evaluate the charge distribution (Table S14) and the bond orders (Table S15) within the {P=C-P(=X)}Pd chelate fragment. The tendencies derived from the computed BO values for the palladium complexes are similar to those presented above on gold complexes (for detailed comparisons, see Tables S11 and S15).

Table S14. Natural charges computed for the atoms contained in the P=C-P(=X)-Pd chelate-backbone, for the series of model {Mes*P=C(Cl)-P(=X)(*i*-Pr)$_2$}PdCl$_2$ complexes.

P=C-P(=X)-Pd backbone	P(III)	C	P(V)	X	Pd
X = O	0.975	-0.950	1.963	-1.066	0.562
X = S	1.026	-0.955	1.396	-0.403	0.415
X = Se	1.034	-0.962	1.294	-0.249	0.387

Table S15. Natural bond orders computed for the atoms within the P=C-P(=X)-Pd backbone, for the {Mes*P=C(Cl)-P(=X)(*i*-Pr)$_2$}PdCl$_2$ complexes involving either P(III)→Pd or X→Pd bonds (X= O, S and Se).

Bond Order	**P=C-P(=O)**					**P=C-P(=S)**				
	P=C	**C-P**	**P=O**	**X→Pd**	**P→Pd**	**P=C**	**C-P**	**P=S**	**X→Pd**	**P→Pd**
total	1.92	1.01	1.00	0.23	0.42	1.86	1.01	1.11	0.42	0.48
covalent	1.33	0.69	0.45	0.05	0.19	1.26	0.74	0.98	0.21	0.22
ionic	0.58	0.33	0.55	0.18	0.23	0.60	0.27	0.13	0.20	0.26

	P=C-P(=Se)				
	P=C	**C-P**	**P=Se**	**X→Pd**	**P→Pd**
total	1.87	1.03	0.99	0.46	0.49
covalent	1.26	0.75	0.85	0.27	0.23
ionic	0.62	0.28	0.13	0.19	0.26

5. References

[1] L. Yang, D. R. Powell, R. P. Houser, *Dalton Trans.,* 2007, **9**, 955-964.
[2] A. Okuniewski, D. Rosiak, J. Chojnacki, B. Becker, *Polyhedron,* 2015, **90**, 47-57.
[3] D. Rosiak, A. Okuniewski, J. Chojnacki, *Polyhedron,* 2018, 146, 35-41.